Correcting the F508del-CFTR variant by modulating eukaryotic translation initiation factor 3–mediated translation initiation

Received for publication, March 28, 2018, and in revised form, July 5, 2018 Published, Papers in Press, July 13, 2018, DOI 10.1074/jbc.RA118.003192

Darren M. Hutt[‡1], **Salvatore Loguercio**[‡1], **Daniela Martino Roth**[‡1,2], **Andrew I. Su**[§], **and William E. Balch**[‡¶3]

From the Departments of [‡]*Molecular Medicine and* [§]*Integrative Structural and Computational Biology and the* [¶]*Skaggs Institute for Chemical Biology, The Scripps Research Institute, La Jolla, California 92037*

Edited by Phyllis I. Hanson

Inherited and somatic rare diseases result from >200,000 genetic variants leading to loss- or gain-of-toxic function, often caused by protein misfolding. Many of these misfolded variants fail to properly interact with other proteins. Understanding the link between factors mediating the transcription, translation, and protein folding of these disease-associated variants remains a major challenge in cell biology. Herein, we utilized the cystic fibrosis transmembrane conductance regulator (CFTR) protein as a model and performed a proteomics-based high-throughput screen (HTS) to identify pathways and components affecting the folding and function of the most common cystic fibrosis–associated mutation, the F508del variant of CFTR. Using a shortest-path algorithm we developed, we mapped HTS hits to the CFTR interactome to provide functional context to the targets and identified the eukaryotic translation initiation factor 3a (eIF3a) as a central hub for the biogenesis of CFTR. Of note, siRNA-mediated silencing of eIF3a reduced the polysome-to-monosome ratio in F508del-expressing cells, which, in turn, decreased the translation of CFTR variants, leading to increased CFTR stability, trafficking, and function at the cell surface. This finding suggested that eIF3a is involved in mediating the impact of genetic variations in CFTR on the folding of this protein. We posit that the number of ribosomes on a CFTR mRNA transcript is inversely correlated with the stability of the translated polypeptide. Polysome-based translation challenges the capacity of the proteostasis environment to balance message fidelity with protein folding, leading to disease. We suggest that this deficit can be corrected through control of translation initiation.

Inherited and somatic rare diseases now encompass greater than 200,000 annotated variants that lead to the loss- or gain-of-toxic function in response to noncoding and coding mutations in the human population (1–3). The onset and progression of these diseases are often caused by misfolding events, which uncouple the affected protein from its community of interacting proteins involved in its biogenesis, stability, degradation, trafficking, and function in the cell, referred to as the proteostasis network (PN)[4] (4–10). The inability of many disease-associated variants to properly interact with their respective proteostasis components results in altered functional profiles leading to the disease phenotype.

Although considerable attention has been focused on post-translational events that control the fold, we are now beginning to appreciate the contribution of co-translational events that manage the numerous folding intermediates associated with the emerging polypeptide chain (9, 11–17). These include the roles of the ribosome in managing the rate of synthesis through codon usage and tRNA abundance and the PN in the co-translational management of the nascent polypeptide chain. What is missing from this broad picture of translational control is the impact of the initiation step, including ribosomal protein availability, on the final protein fold.

To answer the question of whether translation initiation components participate in managing protein folding, we turned to the inherited rare disease cystic fibrosis (CF), which is triggered by point mutations in the cystic fibrosis transmembrane conductance regulator (CFTR) gene, which codes for a cAMP-regulated chloride channel expressed at the apical surface of epithelial cells (18–23). CFTR is generated by co-translational insertion into the endoplasmic reticulum (ER) prior to export to the cell surface where it is responsible for the key steps in the maintenance of proper chloride and bicarbonate balance in the extracellular space of nearly all tissues. Over 70% of CF patients carry at least one allele with a 3-bp deletion (delCTT) resulting in the loss of phenylalanine at position 508 (F508del-CFTR). The resulting F508del-CFTR variant leads to impaired folding and rapid clearance by ER-associated degradation (4, 19, 22, 24–33). The absence of CFTR at the cell surface contributes to loss of hydration of the epithelial lining of the lung and other

This work was supported by National Institutes of Health Grant 5RO1 HL095524 from NHLBI, Grant 2RO1 DK051870 from NIDDK, Grant 5PO1AG049665 from NIA, and by Tobacco-related Disease Research Program Grant 23RT-0012. The authors declare that they have no conflicts of interest with the contents of this article. The content is solely the responsibility of the authors and does not necessarily represent the official views of the National Institutes of Health.

[1] These authors contributed equally to this work.
[2] Present address: Locana, 3210 Merryfield Row, San Diego, CA 92122.
[3] To whom correspondence should be addressed. E-mail: webalch@scripps.edu.

[4] The abbreviations used are: PN, proteostasis network; CFTR, cystic fibrosis transmembrane conductance regulator; CF, cystic fibrosis; HTS, high-throughput screen; hBE, human bronchial epithelial; m.o.i., multiplicity of infection; ER, endoplasmic reticulum; SPN, shortest-path network; YFP, yellow fluorescent protein; siScr, scramble siRNA; NAGA, network-augmented genomic analysis; SAHA, suberoylanilide hydroxamic acid; ALI, air–liquid interface; IP, immunoprecipitation; qRT, quantitative RT; GUS, glucuronidase; AAT, α1-antitrypsin; Z-AAT, Z-variant of AAT; MSR, maladaptive stress response; P/M, polysome/monosome; PIC, protease inhibitor cocktail.

This is an open access article under the CC BY license.

© 2018 Hutt et al. Published under exclusive license by The American Society for Biochemistry and Molecular Biology, Inc.

affected tissues, triggering the progressive clinical pathology characteristic of CF.

The CFTR interactomes of both WT- and F508del-CFTR have been characterized (34, 35), providing insight into the cohort of proteins that mediate CFTR biogenesis and function in the lung. These studies reveal strong differences in the interaction profiles of WT and F508del-CFTR, suggesting that a single point mutation can dramatically alter the community of interactions responsible for its function. These differences allowed us to identify the accelerator of Hsp90 ATPase 1 (Aha1) as a key regulatory proteostasis component mediating the ER retention of the F508del-CFTR disease variant (35, 36). The above data support the importance of proteomic data for the identification of new biological targets responsible for CFTR function. However, recent clinical data have revealed patient to patient variations among individuals carrying the same mutation (22, 37–39), adding a further layer of complexity to our attempts to understand the biogenesis of WT and variant proteins and their impact on disease onset and progression. These observations further emphasize the need for a greater understanding of features that contribute to the nascent synthesis, folding, stability, and trafficking of CFTR variants.

Herein, we present a proteomic approach to uncover pathways and components affecting the folding and function of F508del-CFTR in human disease. A specific siRNA library (2569 siRNAs) was used to screen bronchial epithelial cells to identify PN components that can be targeted to restore cell-surface F508del-CFTR channel activity. The PN hits were mapped to the CFTR interactome (34), using a novel shortest-path network (SPN) approach, to characterize the mechanism of correction for non-CFTR interacting hits and to prioritize targets of interest for correcting the basic defect associated with the F508del variant. This function-based analysis identified the eukaryotic translation initiation factor 3a (eIF3a) (9, 11–13, 40–49) as the top target for siRNA-mediated functional correction of F508del-CFTR in bronchial epithelial cells. We show that the reduced expression of eIF3a provides a more optimal environment for correction of not only F508del-CFTR but also other CFTR variants spread across the sequence, suggesting that protein translational events dependent upon eIF3 in general and eIF3a specifically serve as regulatory elements for generating the genome to proteome transformation responsible for CF biology. The identification of this target suggests that translational initiation is suboptimal in the mRNA of variants leading to a disconnect with proteostasis-mediated events involved in CFTR folding. Subtle adjustments to the eIF3 machinery could provide a more global approach to redirect the processes governing transformation of the genomic state to a functional proteomic state leading to improved patient health in the clinic.

Results

siRNA-based proteostasis screen

Given the central importance of proteostasis in co- and post-translational folding of CFTR, we performed an siRNA high-throughput screen (HTS) using a library composed of 2569 siRNAs targeting individual PN components, including the translational machinery, cytosolic and ER luminal chaperones, the degradation system, and post-translational regulatory proteins (Fig. 1*A* and Information S1). The library was composed of four siRNA sequences per target, and the screen was performed in triplicate. The HTS was performed in the bronchial epithelial cell line, CFBE41o− (referred to herein as CFBE), engineered to express both the ER-restricted F508del-CFTR as well as a halide-sensitive YFP variant (H148Q/I152L). The fluorescence of YFP-H148Q/I152L is quenched in the presence of halide ions, such as external iodide (50), which can be taken up by cells only in the presence of a functional cell-surface F508del-CFTR channel. In this assay, silencing of PN components that restore trafficking and function to the F508del variant at the cell surface will allow influx of external iodide upon activation of the CFTR channel with forskolin and genistein leading to increased YFP quenching.

The screen identified 456 PN components whose silencing led to a statistically significant ($p < 0.05$) increase in YFP quenching relative to treatment with a negative control siRNA (siScr). Of these, 89 siRNAs caused a greater than 25% decrease in basal YFP fluorescence ($p < 0.05$), which can be attributed either to a decrease in cell number, due to toxicity, or a disruption of global protein folding leading to reduced YFP expression. Because both the loss of global protein folding or cell viability are undesirable, these targets were eliminated from future consideration, leaving us with a target list of 367 PN components (Fig. 1*B* and Information S2), a hit rate of 14.3%. We noted that only 73 out of 367 siRNA hits are CFTR-interacting proteins, based on the published CFTR interactome generated using the same CFBE model system (Fig. 1*C*) (34), raising the question of how the remaining 294 siRNA hits are mediating correction of F508del-CFTR.

Using network-augmented genomic analysis to identify folding management hubs

We developed a novel algorithm to address how these non-CFTR interacting, siRNA hits are connected to CFTR, which we called network-augmented genomic analysis (NAGA). We first expanded the CFTR Interaction NetworK (CINK) from its 576 proteins, as characterized in the CFTR interactome (34). To accomplish this, we utilized publicly available protein interaction databases (see under "Experimental procedures") to assemble an undirected network of human protein interactions. For each interaction, a confidence score was calculated (see under "Experimental procedures"), reflecting the reliability of its combined experimental evidence, providing weight to the CINK, where more reliable interactions are favored during a shortest path analysis. With this platform, the task of connecting the 367 siRNA hits (sources) to CFTR (target) was formulated in terms of a single-source shortest-path problem for a graph, and thus efficiently solved with the Dijkstra's algorithm (51) to generate the final shortest-path network. We next computed the number of siRNA hits that utilize a given CFTR-interacting protein on its shortest path to interface with CFTR (Fig. 2*A*). CFTR-interacting proteins that connected two or more siRNA hits (*N*-specific (N_{sp})) to CFTR were classified as hub proteins. To filter out nonspecific protein hubs (*i.e.* proteins whose high-connectivity values are mostly related to the

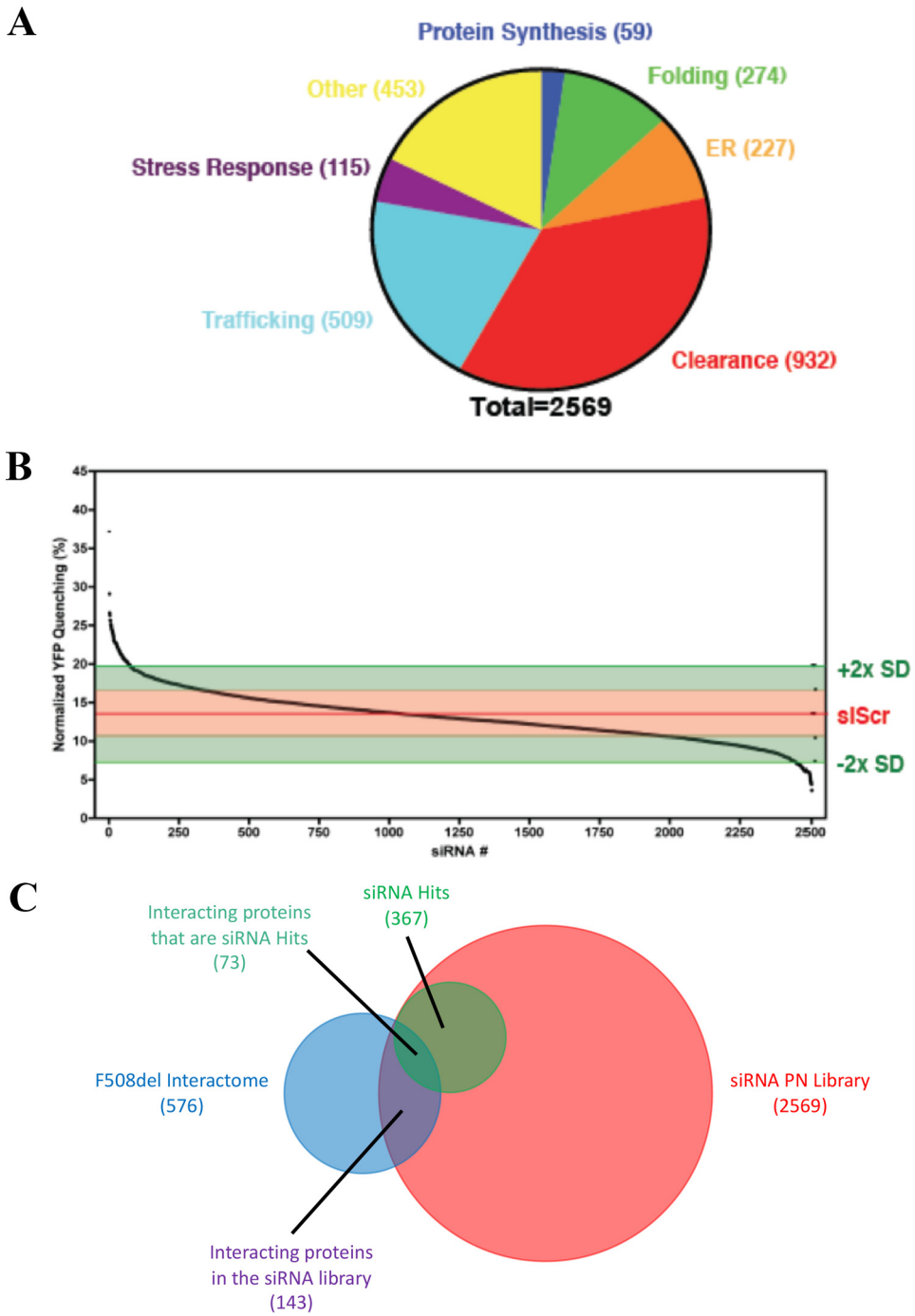

Figure 1. High-throughput screening of proteostasis siRNA library. *A, pie chart* summarizing the gene ontology pathway assignment of proteostatic siRNA targets. *B,* scatter plot summarizing the YFP quenching data for the high-throughput siRNA screen. The *red band* represents the YFP quenching for the siScr with its associated error, and the *green bands* represent the 2-fold standard deviation range for the percent of YFP quenching relative to the siScr. *C, Venn diagram* depicting the number of proteins in the expanded CFTR interactome, the siRNA library, and high-throughput hit list.

siRNA library composition and the topology of the graph), the SPN computation was repeated using a random selection of 367 targets from the siRNA library and iterated 1000 times. Using this approach, a "hubness" value for specific (N_{sp}) and nonspecific (N random (N_{rdm})) siRNA target lists was determined for each hub protein.

Using SPN, we mapped 358 of the 367 HTS hits to the expanded CINK, revealing a sub-network of 525 proteins and 3548 interactions, with a significant presence of community structure (p = 5.6E10−9, see "Experimental procedures"). A total of 196 proteins connected the 358 HTS hits to CFTR, with 119 of these interacting directly with CFTR. Of these, we identified 70 proteins that linked two or more F508del-correcting HTS hits ($N_{sp} \geq 2$). After filtering for nonspecificity of these hub proteins, we identified 41 proteins that exhibited a $N_{sp} \geq 2$ and a N_{sp}/N_{rdm} ratio >2 (Fig. 2*B*; Table 1). We estimated a false discovery rate (FDR) of 0.02 for these filtering criteria (see under "Experimental procedures"). A further examination of

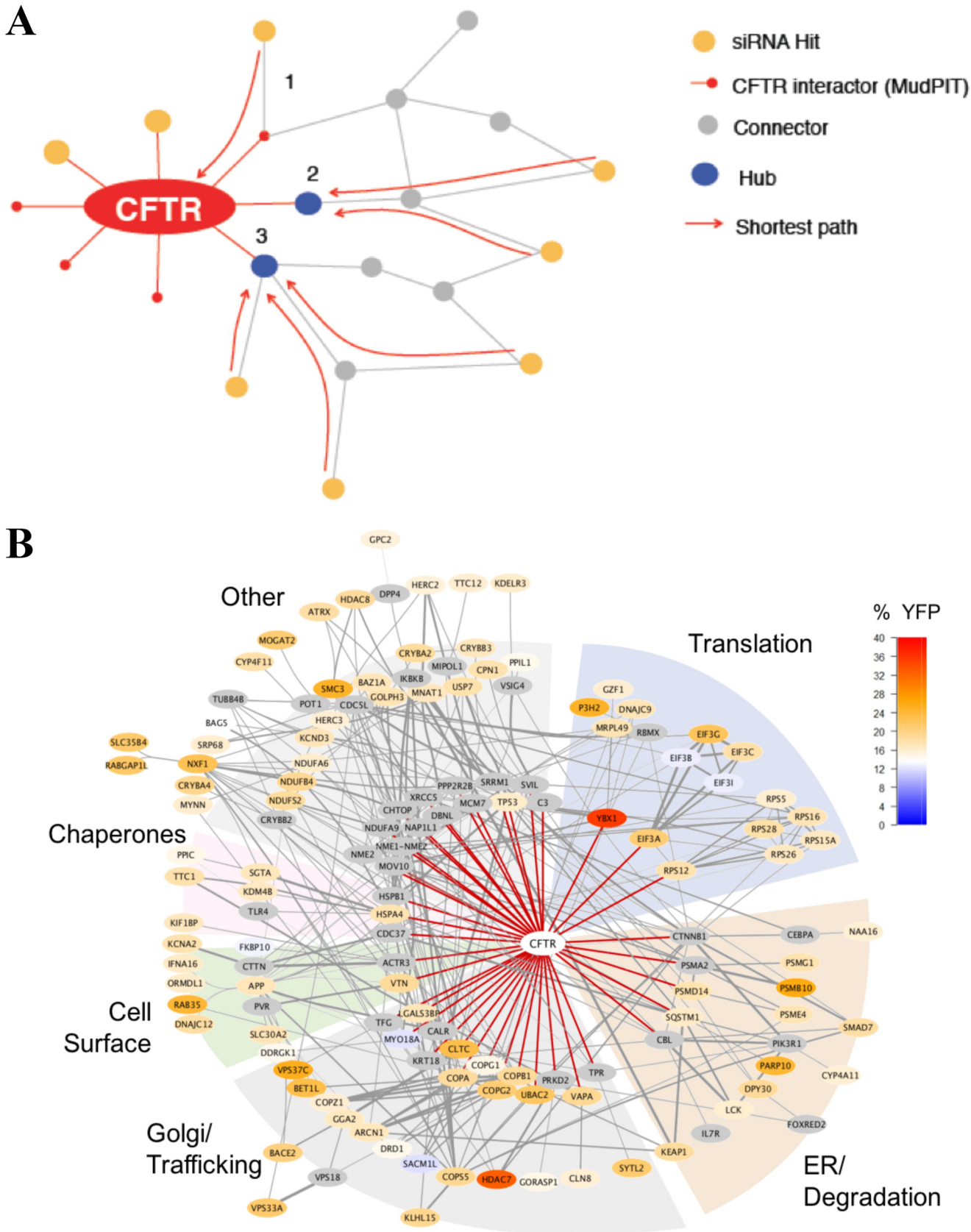

Figure 2. Shortest path analysis of high-throughput screening hits identify hub proteins for connectivity to CFTR. *A,* diagram explaining the shortest path analysis approach and the defining hub proteins. *B,* network map depicting the connectivity of high-throughput hits to CFTR. The nodes with a *black border* represent the hub proteins from the NAGA algorithm. The nodes are color-coded based on the level of YFP quenching in the CFTR functional assay. The proteins in the network are arranged according to their predicted subcellular localization or cellular function.

Table 1

Shortest path analysis reveals Hub proteins connecting siRNA targets, which correct F508del-CFTR to CFTR-interacting proteins

The table depicts the gene name, EID, the number of corrective siRNA targets connecting to the indicated hub protein (N_{sp}), the number of random siRNAs from the proteostasis siRNA library connecting to the indicated hub protein (N_{rnd}), the N_{sp}/N_{rnd} ratio, the relative affinity of the indicated hub protein for WT- and F508del-CFTR as determined in the expanded CFTR interactome, and the percent of YFP quenching, S.D., and p value determined from the HTS screen.

					CFTR Core interactome binding		HTS Screen		
	EID	Nsp	Nrnd	Nout/Nrnd	Interaction(wt)	Interaction(D508F)	%YFP	SD	P value
EIF3A	8661	5	1.42	3.52	NA	0.51	20.45	2.43	0.00002
PSMA2	5683	4	1.18	3.39	NA	0.65	14.02	0.62	0.47
NME2	4831	3	1.06	2.84	NA	NA	NA		
HSPA4	3308	9	3.71	2.42	0.40	0.57	17.26	4.29	0.01
SRRM1	10250	7	3.18	2.20	0.14	0.49	NA		
TPR	7175	4	1.84	2.17	NA	0.391	NA		
CUL1	8454	4	1.90	2.10			12.01	0.48	0.5
XRCC5	7520	3	1.46	2.05	0.43	0.57	NA		
HSPA5	3309	6	2.95	2.03	0.23	0.40	17.55	2.41	0.02
CTNNB1	1499	4	1.98	2.02	0.46	0.61	NA		
KDELR2	11014	2	0.16	12.20	NA	0.25	17.08	0.17	0.004
SIRT7	51547	2	0.17	11.76			17.74	2.54	0.02
ARCN1	372	2	0.17	11.63	NA	NA	20.35	2.19	0.03
GGA2	23062	2	0.17	11.63			16.58	0.52	0.02
TNS3	64759	2	0.18	10.99	NA	0.66	11	1	0.7
CDC5L	988	2	0.31	6.51	NA				
CRYBB2	1415	2	0.34	5.93			6.17	3.38	0.0002
MYO18A	399687	2	0.38	5.29	NA	0.48	14.10	3.32	0.47
PRKD2	25865	2	0.50	3.97	NA	NA	NA		
LGALS3BP	3959	2	0.51	3.95	0.27	0.38	16.86	0.88	0.01
CBL	867	2	0.53	3.80	NA	NA	15.09	1.8	0.09
UBE2L3	7332	2	0.53	3.77			19.46	2.31	0.001
MAP1LC3B	81631	2	0.56	3.60			22.10	5.3	0.0000003
UBTF	7343	2	0.65	3.08	NA	NA	NA		
COPG2	26958	2	0.71	2.81	NA	NA	18.32	1.45	0.001
PGRMC1	10857	2	0.73	2.75	0.32	0.52	12.50	1.09	0.3
MNAT1	4331	2	0.73	2.74			16.66	2.62	0.003
ARL1	400	2	0.84	2.39	0.32	0.31	11.37	2.28	0.3
PHB	5245	2	0.88	2.28	NA	0.39	11.67		
COPA	1314	2	0.88	2.27	NA	0.39	21.96	3.24	0.0004
TFG	10342	2	0.88	2.26	NA	NA	NA		
MCM7	4176	2	0.92	2.17	0.58	0.65	NA		
VTN	7448	2	0.93	2.16	NA	0.31	18.46	0.93	0.03
COPB1	1315	2	0.96	2.08	NA	0.25	18.46	0.53	0.0008
PPP2R2B	5521	2	0.99	2.02	NA	0.25	NA		

these 41 hub proteins revealed that 24 of them were recovered in the CFTR interactome and that 22 of these CFTR-interacting hubs exhibited an increased binding affinity for F508del-CFTR relative to WT-CFTR (log10(WT/F508del) ≤0.5; p value 0.038) (Table 1) (34). Further analysis revealed that 25 of the 41 hub proteins were targeted in the siRNA HTS screen where 19 of them provided functional correction of F508del-CFTR, yielding a hit rate of 76%. These data highlight the power of SPN in improving and understanding combined siRNA and MS datasets (Table 1).

Assessing the role of SPN hits

To understand the importance of all the SPN hubs, we tested the impact of siRNAs targeting 10 of the 16 hub proteins not previously tested in our siRNA HTS screen (Table 1) to assess their ability to correct F508del-CFTR. We observed that the silencing of seven of these proteins led to a statistically significant ($p < 0.05$) increase in F508del-CFTR function (Table 2). These results reveal that the silencing of 26 of the 35 hub proteins tested resulted in restoration of a functional F508del-CFTR at the cell surface of CFBE cells, which supports our selection strategy for network connectivity using NAGA, defining, for the first time, a functional interaction community of proteins managing F508del in human disease.

Of the many interactions detected, the hub with the best combined N_{sp} and N_{sp}/N_{rdm} ratio was the eIF3a (Table 1). Our analysis revealed that, in addition to being a hit in the siRNA screen itself, five other HTS hits ($N_{sp} = 5$) (eIF3b, -c, -g, -i, and -l as well as eIF5a) were connected to F508del-CFTR through our SPN analysis (Fig. 2*B*). The hubness of eIF3a was not due to

Table 2

YFP quenching data for siRNA knockdown of hub proteins not previously tested in the HTS screen

The percent of quenching of YFP-H148Q/I152L in F508del-expressing CFBE cells ± S.D. ($n = 3$; p value determined using two-tailed t-test using siScr as the reference).

siRNA	% Quench	SD	P Value
siScr	12.52	2.33	
siMCM7	21.74	2.03	0.01
siXRCC5	9.85	0.76	0.13
siPRKD2	16.52	0.70	0.05
siSRRM1	15.50	1.34	0.13
siPPP2R2B	17.58	3.23	0.09
siTPR	17.72	1.36	0.03
siCTNNB1	17.49	1.11	0.03
siNME2	18.62	1.35	0.02
siCDC5L	23.37	0.65	0.001
siTFG	17.89	1.39	0.03

a preponderance of nonspecific interactions because its randomized connectivity score was low ($N_{rdm} = 1.4$) (Table 1). The identification of eIF3a as the top hub for the correction of F508del-CFTR was consistent with our observation for the enrichment of factors involved in the protein synthesis in our hit list from the HTS, where 15 of 59 potential targets resulted in the functional correction of F508del-CFTR, a hit rate of 25.4%, by far the highest among all PN categories in our siRNA library (Table 3). Additionally, a number of protein synthesis components were recovered in the interactome and exhibit an increased affinity for F508del- relative to WT-CFTR, including YBX-1, PABPC1, and UPF1 (34). These data suggest that the translation machinery may play an unanticipated role in the inability of cells to fold the F508del variant and that modulation of this machinery could provide functional correction of F508del-CFTR at the cell surface, consistent with the recent observation that the silencing of ribosomal protein L12 (RPL12), which plays a role in translation elongation, can improve stability, trafficking, and function of F508del CFTR (52).

Silencing of eIF3a corrects the basic defects of F508del-CFTR

To establish a functional role for eIF3a and possibly other eIF3 family members in the biogenesis of F508del-CFTR, we used siRNA to target all 13 members of the eIF3 family (a–m) and analyzed the impact on F508del-CFTR stability and trafficking. Silencing of most eIF3 family members, with the exception of eIF3d, eIF3f, and eIF3j, resulted in a significant increase in the amount of ER-localized F508del-CFTR (band B) (Fig. 3, *A* and *B*), suggesting that the *de novo* fraction of F508del-CFTR synthesized in an environment with a reduced pool of functional eIF3, and therefore 43S PIC, exhibited increased stability. We also observed correction of the F508del-CFTR trafficking and an improved trafficking index (C/B ratio, where C/B ratio = ratio of the level of band C glycoform to the level of band B glycoform) in response to the silencing of eIF3a, -c, -e, -g, -h, -i, -k, -l, and -m (Fig. 3, *A* and *B*). The trafficking index reflects improved efficiency of export from the ER where band C is the post-ER glycoform and band B is the steady-state population of F508del-CFTR found in the ER. Only the silencing of eIF3b yielded a stabilized F508del-CFTR that is not recognized for export, a surprising result given that both eIF3a and -b represent the nucleation core for the assembly of the eIF3 holocomplex (48). It is possible that the eIF3b did not achieve the necessary knockdown (KD) to correct the trafficking defect despite increasing the stability of F508del-CFTR, a question that will require further attention in future studies. These data suggest that the fraction of F508del-CFTR exhibiting increased stability is also recognized as an exportable fraction for trafficking to the cell surface, with the silencing of eIF3a providing the most robust correction of F508del-CFTR. We observed a similar effect on F508del-CFTR stability and trafficking with the eIF3-interacting proteins eIF4g1 (53), eIF4g2 (54, 55), eIF5a (56), and eIF2a (Fig. 3*A*) (12, 13, 43, 45). These data suggest that events associated with translation initiation in general and eIF3a specifically are not conducive to the folding of F508del-CFTR.

Table 3

Analysis of high-throughput YFP quenching data reveals enrichment of PN categories

Data depict the represented PN categories, the number of siRNA targets in each category (PN library), corrective siRNA from the HTS YFP assay (hits), percent of total, and p value for enrichment.

PN Category	PN library	Hits	% of Total	p-value
Protein synthesis	59 (2.3%)	15 (4.1%)	25.4	0.0165
Folding	274 (10.7%)	58 (15.7%)	21.2	0.0008
ER	227 (8.8%)	44 (11.9%)	19.4	0.0179
Stress response	115 (4.5%)	21 (5.7%)	18.3	0.1401
Trafficking	509 (19.8%)	75 (20.3%)	14.7	0.4185
Other	454 (17.7%)	52 (14.1%)	11.5	0.9804
Clearance	932 (36.3%)	104 (28.2%)	11.2	0.9998

sieIF3a corrects the stability, trafficking, and function of multiple CFTR variants

Because we observed that eIF3a silencing provided the most robust correction of the trafficking defect associated with F508del variant, we investigated whether additional disease variants would also be corrected by eIF3a silencing. We selected three additional CFTR variants, G85E, R560T, and N1303K, that could provide positional effects, given their location in the N terminus, NBD1, and NBD2 domains, respectively. These three variants also exhibit a strong ER retention profile at steady state (Fig. 3*C*). Intriguingly, all three variants exhibited a robust increase in band B expression levels as well as a robust increase in band C in response to the silencing of eIF3a (Fig. 3*C*), confirming that a partial reduction of the cellular level of eIF3a generates an environment that is permissive to the folding of CFTR variants located across the entire length of polypeptide chain, suggesting a general mechanism for the improved stability and folding rather than a variant-specific one.

eIF3a suppression restores chloride conductance

Because we observed correction of F508del-CFTR trafficking in response to the silencing of numerous eIF family members, we wanted to assess whether the band C fraction represented a cell-surface–localized, functional chloride channel. For this

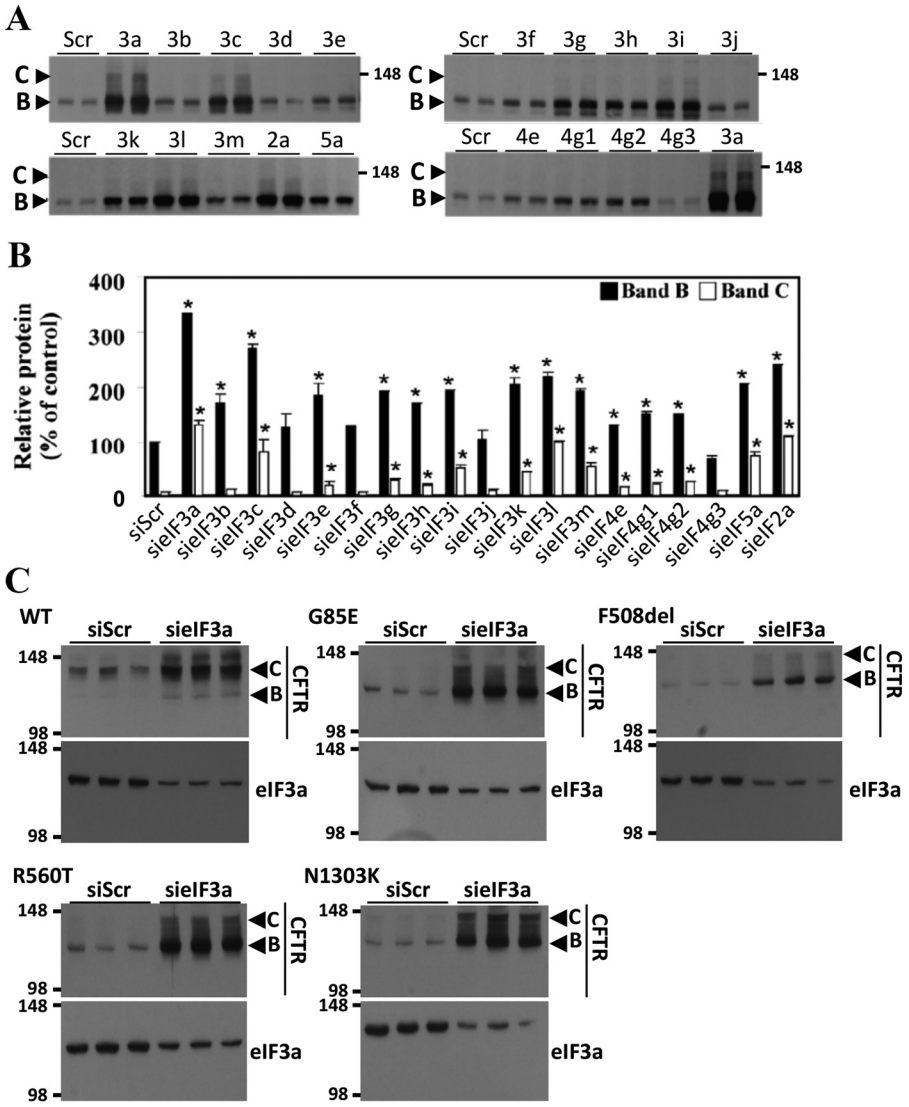

Figure 3. Silencing of members of the eukaryotic translation initiation factor family rescue F508del-CFTR function. *A,* immunoblots of F508del-CFTR ER (*band B*) and post-ER (*band C*) glycoforms following silencing of eIF proteins. *B,* quantification of the immunoblot in *A*. Data are normalized to the amount of band B glycoform in the siScr control and represent mean ± S.D., $n \geq 3$, and * indicates $p \leq 0.05$ relative to the same glycoform for siScr. *C,* immunoblot of the indicated CFTR variants and eIF3a following the silencing of eIF3a.

purpose, we utilized the YFP-quenching assay employed in the siRNA HTS (50). We observed that the silencing of eIF3a–c, -g, -i, and -l as well as eIF5a mediated the functional correction of the F508del-CFTR disease variant (Fig. 4*A*) with eIF3a again providing the most robust correction, reaching a level of YFP quenching similar to that seen with siHDAC7, a validated target known to increase F508del cell-surface function in CFBE41o− cells (57). The observation that eIF3b provided a modest functional correction to F508del-CFTR despite the lack of band C (Fig. 3, *A* and *B*) suggests that either the level of trafficking correction is below our detection limit or that differences in the KD efficiency between the experiments contributed to this discrepancy. To assess whether the increase in YFP quenching seen in response to sieIF3a in CFBE cells contributes to restoration of a functional F508del-CFTR channel at the cell surface, we monitored the sensitivity of this quenching reaction to the CFTR-specific channel inhibitor, CFInh172. The presence of the CFTR inhibitor blocked the YFP quenching seen with sieIF3a (Fig. 4*B*), supporting our conclusion that the partial knockdown of eIF3a leads to functional recovery of the F508del-CFTR disease variant at the cell surface.

We also examined the impact of combining eIF3a silencing with Vx809 or suberoylanilide hydroxamic acid (SAHA), known small molecule correctors of F508del-CFTR (57, 58), to monitor whether a further improvement in the functional rescue of F508del-CFTR could be observed. Combining the treatment of 3 μM Vx809 or 1 μM SAHA with sieIF3a led to a significant improvement in the functional correction of F508del-CFTR than that seen with any of the three treatments alone (Fig. 4*C*). These data provide evidence that the silencing of eIF components, particularly eIF3a, have a marked effect on F508del functional rescue, suggesting that events regulated by the eIF3 holocomplex manage the ability of CFTR variants to achieve a functional fold.

To investigate whether other diseases of protein folding are sensitive to modulation of the eIF3a expression level, we tested

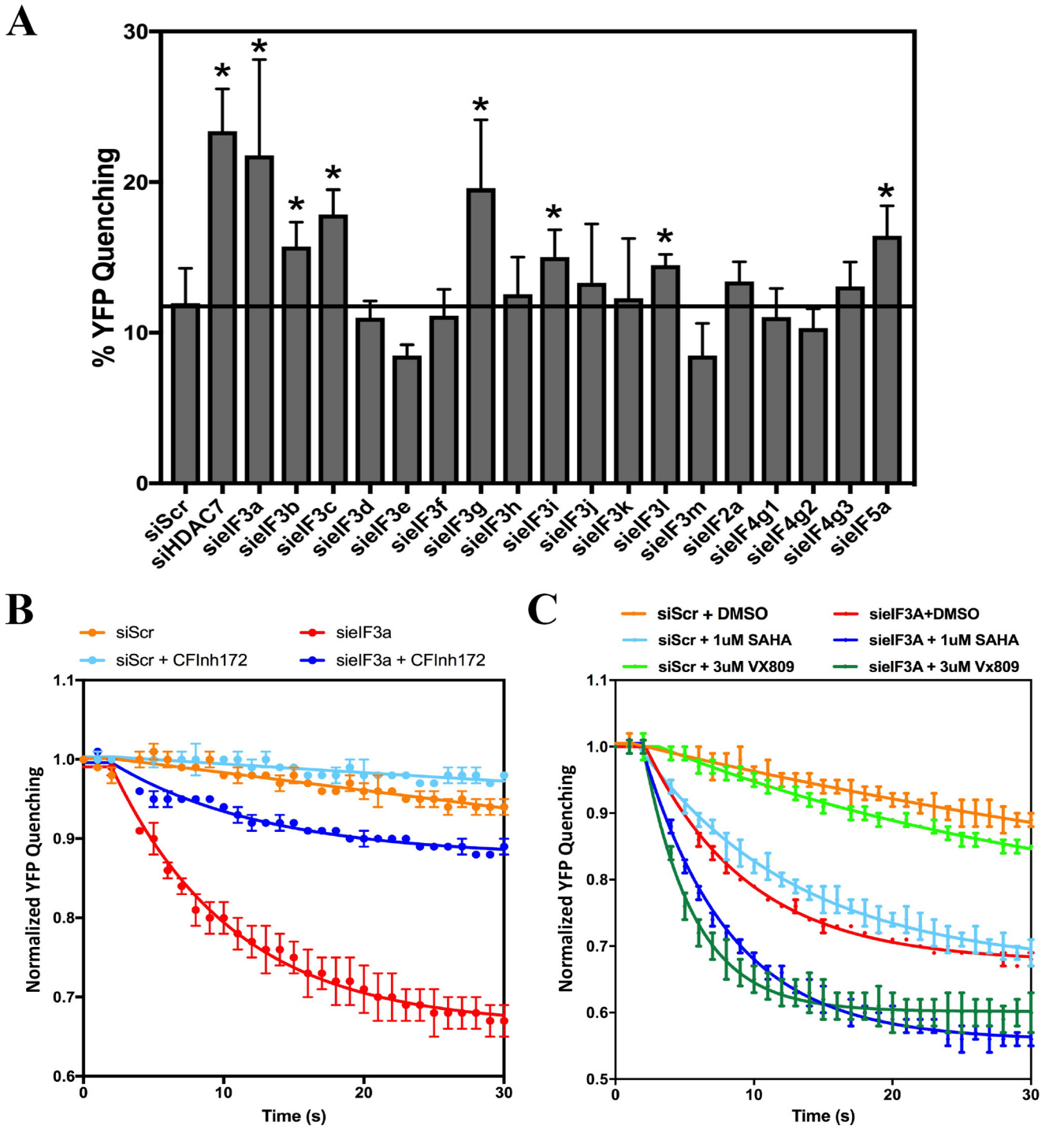

Figure 4. Silencing of eIF3 subunits restores function of F508del-CFTR in CFBE cells. *A, histogram* showing the percentage of YFP-H148Q/I152L quenching in F508del-expressing CFBE–YFP cells transfected with the indicated siRNA for 72 h (HDAC7 siRNA was used as positive control). Data represent the mean ± S.D., $n \geq 3$, and * indicates $p < 0.05$ relative to control. *B,* scatter plot showing YFP fluorescence quenching in F508del-expressing CFBE–YFP cells transfected with scramble or eIF3a siRNA in the presence or absence of the CFTR-specific inhibitor, CFInh172. *C,* scatter plot showing the YFP fluorescence quenching in F508del-expressing CFBE–YFP cells treated with scramble siRNA + DMSO (*red*), eIF3a siRNA + DMSO (*orange*), 1 μM SAHA (*blue*), sieIF3a + 1 μM SAHA (*cyan*), 3 μM Vx809 (*dark green*), or sieIF3a + 3 μM Vx809 (*light green*). The data in *B* and *C* are shown as relative YFP fluorescence normalized to the $t = 0$ for each condition and fit as plateau with exponential decay and represent the mean ± S.D., $n = 3$.

the effect of eIF3a silencing in a cellular model of α1-antitrypsin deficiency, expressing the Z-variant of α1-antitrypsin (AAT) (Z-AAT), an ER-restricted variant of the secreted AAT protein. Z-AAT accumulates as a misfolded polymer in the ER compartment (59, 60). Intriguingly, although silencing of eIF3a did not improve the expression of the immature ER glycoform or maturation of the Z-variant nor an increase in the secretion of Z-AAT, changes were seen with sieIF3k and sieIF3l (Information S3). These data are consistent with previous observations that eIF3a might affect the translation of a specific set of mRNAs (61, 62) and raise the possibility that translation events platformed by eIF3a play differential roles in tuning different

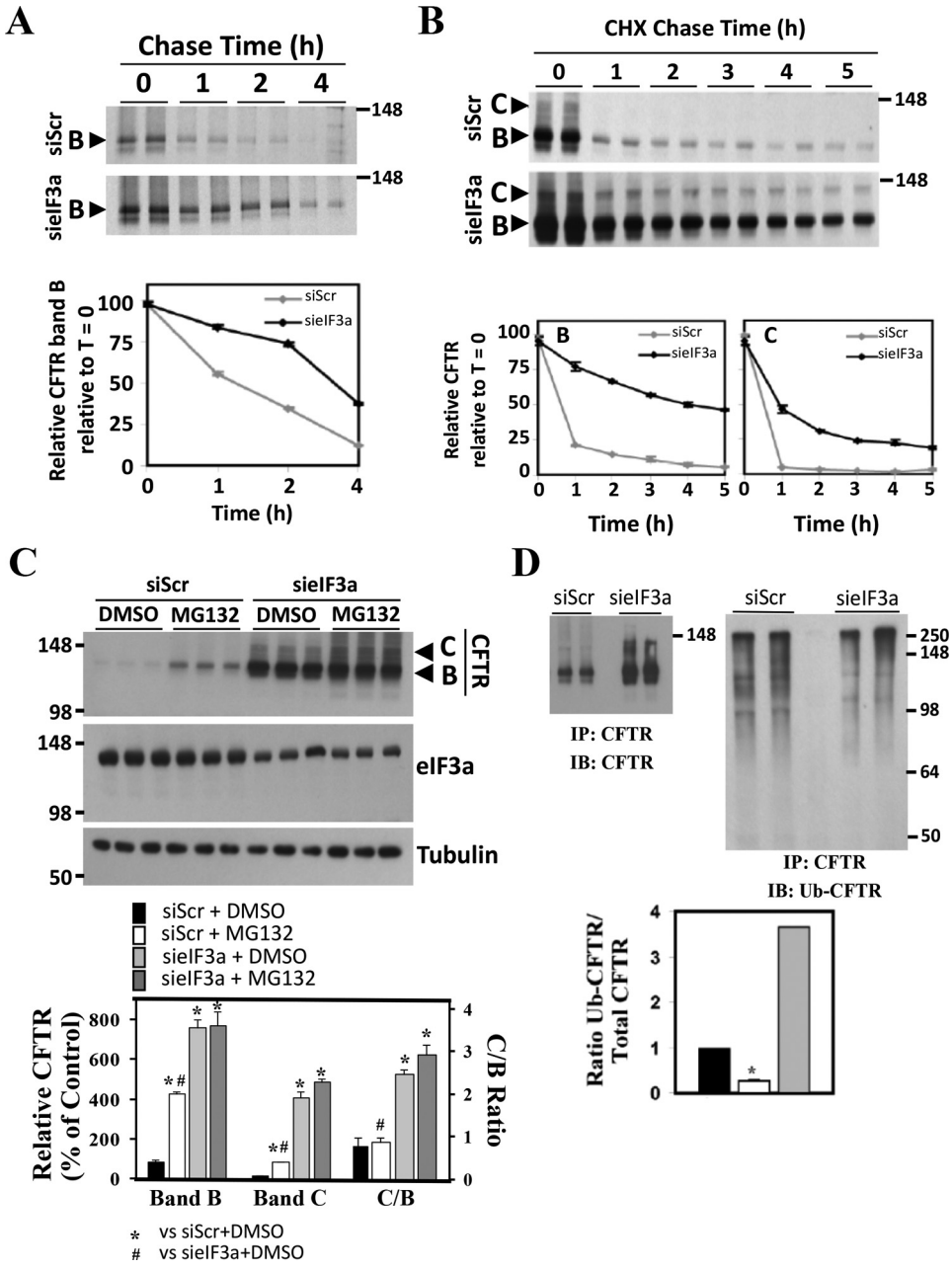

Figure 5. eIF3a silencing restores F508del-CFTR stability of bands B and C pools. *A,* pulse–chase analysis of F508del-CFTR in response to sieIF3a treatment. The quantification is shown as a percent of F508del-CFTR band B at time 0 ($t = 0$) (mean ± S.D., $n \geq 2$). *B,* immunoblots of F508del-CFTR band B and band C glycoforms during cycloheximide (*CHX*) chase following treatment with scramble or siEIF3a siRNA. Quantification data are shown as a percent of F508del-CFTR band B and band C at time 0 ($t = 0$) (mean ± S.D., $n \geq 2$). *C,* immunoblots of CFTR and eIF3a in response to sieIF3a treatment in combination with DMSO or the proteasomal inhibitor MG132 (10 μM for 5 h) in F508del-CFTR–expressing CFBE cells. *Histogram* shows the quantitative analysis of F508del-CFTR glycoforms (*bands B* and *C*) under the indicated conditions. Results were normalized to a percent of the control siRNA signal for the CFTR band B. Results are shown as a mean ± S.D., $n \geq 3$, and *p* values were determined by two-tailed *t* test using the indicated condition as reference point; * or # indicate $p < 0.05$. *D,* immunoblots (*IB*) of total and ubiquitinated CFTR (*poly-Ub*) in CFTR immunoprecipitates (*IP:CFTR*) in response to sieIF3a treatment of F508del-CFTR–expressing cells ($CFTR^{-/-}$ cells lacking CFTR were used as negative control for CFTR IP). Quantification of CFTR ubiquitination is shown, as a ratio of ubiquitin to total CFTR, and the control siRNA is set to 1.

mRNA species for productive protein production (9, 12, 13, 16, 45).

Silencing of eIF3a increases F508del-CFTR stability

Given that the eIF3 complex has been shown to interact with the proteasome machinery (63) to facilitate the degradation of unstable nascent polypeptides, we tested whether silencing of eIF3a would affect F508del-CFTR degradation using a pulse–chase analysis of F508del-CFTR in response to sieIF3a. Consistent with its effects on improving trafficking and function, eIF3a silencing markedly reduced the degradation of F508del-CFTR (Fig. 5*A*). Because the trafficking kinetics and destabilized nature of F508del-CFTR make it difficult to detect band C on pulse–chase experiments, we used a cycloheximide chase to monitor the stability of the band C glycoform generated in response to the silencing of

eIF3a. Consistent with the increased appearance of band B, we also observed increased stability of band C in response to cycloheximide-mediated inhibition of *de novo* protein synthesis relative to that seen with temperature-rescued (30 °C) band C chased at 37 °C (Fig. 5*B*). Here, increased F508del-CFTR C band stability was possibly due to alterations in proteasome-mediated degradation and/or improved folding impacted by either mitigation of translation events associated with the mutant F508del mRNA or by providing a more stable physiological state in which to achieve a more functional fold.

To address the latter possibility, we combined the proteasome inhibitor, MG132, with sieIF3a treatment. Whereas both MG132 treatment and sieIF3a led to an increase in the expression of band B and correction of trafficking to band C (Fig. 5*C*), only the silencing of eIF3a resulted in an improved trafficking index (C/B). Combining these two treatments did not result in an improvement on F508del-CFTR stability or trafficking (Fig. 5*C*), suggesting that functional disruption of translation events managed by eIF3a affects co-translational and/or post-translational folding of F508del-CFTR such that the variant is no longer heavily degraded by the proteasome. This hypothesis is supported by the observation that the level of ubiquitinated CFTR (Ub-CFTR) increases almost 4-fold in response to MG132 treatment, whereas it decreases almost 4-fold in response to the silencing of eIF3a (Fig. 5*D*). These results highlight that correction of F508del-CFTR by modulation of the translational process is not due to impaired proteasome degradation and could reflect a direct or indirect role for translational events in the productive generation of the CFTR polypeptide.

eIF3a silencing reduces the rate of translation of F508del-CFTR

Because eIF3a is an important component of the eIF3 holocomplex (43, 48, 64, 65), we monitored the impact of eIF3a silencing on the polysome profile of CFBE cells. Silencing of eIF3a resulted in a significant decrease in the number of polysomes and a concomitant increase in the level of 80S monosomes in CFBE cell lysates (Information S4), consistent with previous observations in response to the silencing of eIF3a and most other eiF3 subunits in mammalian cells (43, 48). The reduced polysome to monosome (P/M) ratio seen for sieIF3a in HEK293 and HeLa cells correlated with a reduction in the rate of translation initiation (43, 48), raising the possibility that eiF3a KD might also alter the rate of translational initiation or number of initiation events on the F508del mRNA. To address this possibility, we performed a ^{35}S-pulse–labeling time course to monitor the rate of [^{35}S]Met incorporation in *de novo*-synthesized F508del-CFTR. We observed a robust increase in the level of ^{35}S-labeled F508del-CFTR (Fig. 6*A*), possibly suggesting an overall increase in translation in response to the silencing of eIF3a. We have previously shown that the increased expression of F508del-CFTR and other disease-associated protein variants activates a heat-shock–like chronic stress condition, termed the maladaptive stress response (MSR), which reduces the correctability of F508del-CFTR (66), suggesting that simply increasing the expression of F508del would not remediate the defects associated with this disease-associated variant. To address this potential discrepancy, we sought to address whether the silencing of eIF3a also altered the expression level of CFTR mRNA, as a potential source for the observed increase in F508del-CFTR translation. We did observe an sieIF3a-mediated 3.3-fold increase in the amount of F508del-CFTR mRNA levels in CFBE cells relative to that seen in control siRNA-treated cells (Fig. 6*B*). When the total pool of mRNA available for translation was considered in the analysis of ^{35}S-labeled *de novo*-synthesized F508del-CFTR, we actually observed a 2.2-fold decrease in the amount of F508del-CFTR protein produced per mRNA molecule in response to the silencing of eIF3a (Fig. 6*C*).

To address whether the reduced CFTR production was the result of a general decrease in protein translation, as suggested previously (43, 48), we performed a 1-h ^{35}S pulse-labeling of F508del-CFTR– expressing CFBE cells treated with control or eIF3a siRNA, and we analyzed the amount of total protein labeled relative to that seen in WT-CFTR– expressing CFBE cells. We observed that F508del-CFTR– expressing CFBE cells exhibited a 60% decrease in total protein translation compared with CFBE cells expressing WT-CFTR (Fig. 6*E*). This observation is in agreement with the chronic heat shock-like stress (MSR) seen in F508del-expressing cells (66), where inhibition of *de novo* protein synthesis is a known consequence of activation of the heat-shock response. Intriguingly, the silencing of eIF3a in F508del-CFTR– expressing CFBE cells resulted in the restoration of a more WT-like translation profile, approaching 80% of that seen in WT-expressing CFBE cells (Fig. 6*E*). Moreover, comparing the total labeled protein content between WT-expressing and sieIF3a-treated F508del-expressing CFBE reveals a 20% reduction, which is consistent with previous reports assessing the impact of eIF3a knockdown (67). To confirm this observation, we determined the steady-state protein levels per cell in CFBE cells treated with control or eIF3a siRNA relative to that seen in WT-CFTR– expressing cells. Consistent with the results of the pulse-labeling experiment, we observed that F508del-CFTR– expressing CFBE cells yielded a protein expression level of 150 pg of total protein per cell, a 50% reduction compared with WT-expressing CFBE cells where a protein expression level of 300 pg/cell was detected (Fig. 6*D*). Strikingly, silencing of eIF3a restored the protein expression level to 240 pg/cell, a correction to a level 80% of WT-expressing cells (Fig. 6*D*).

sieIF3a improves F508del function on primary patient–derived epithelium

Because eIF3a silencing results in restoration of a functional cell-surface pool of F508del-CFTR in CFBE cells, we addressed whether this result could be recapitulated in patient-derived primary bronchial epithelia (hBE) homozygous for the F508del mutation (F508del/F508del). The adeno-shRNA–mediated silencing of eIF3a in primary F508del-hBE cells resulted in a stabilization of the ER-localized band B fraction as well as a correction of the trafficking defect associated with this mutation as determined by the appearance of band C (Fig. 7, *A* and *B*, *sheIF3a 500 and 1000 m.o.i.*). The correction of F508del-CFTR was observed despite only a modest silencing of eIF3a in these human primary airway cells. The restored band C level sur-

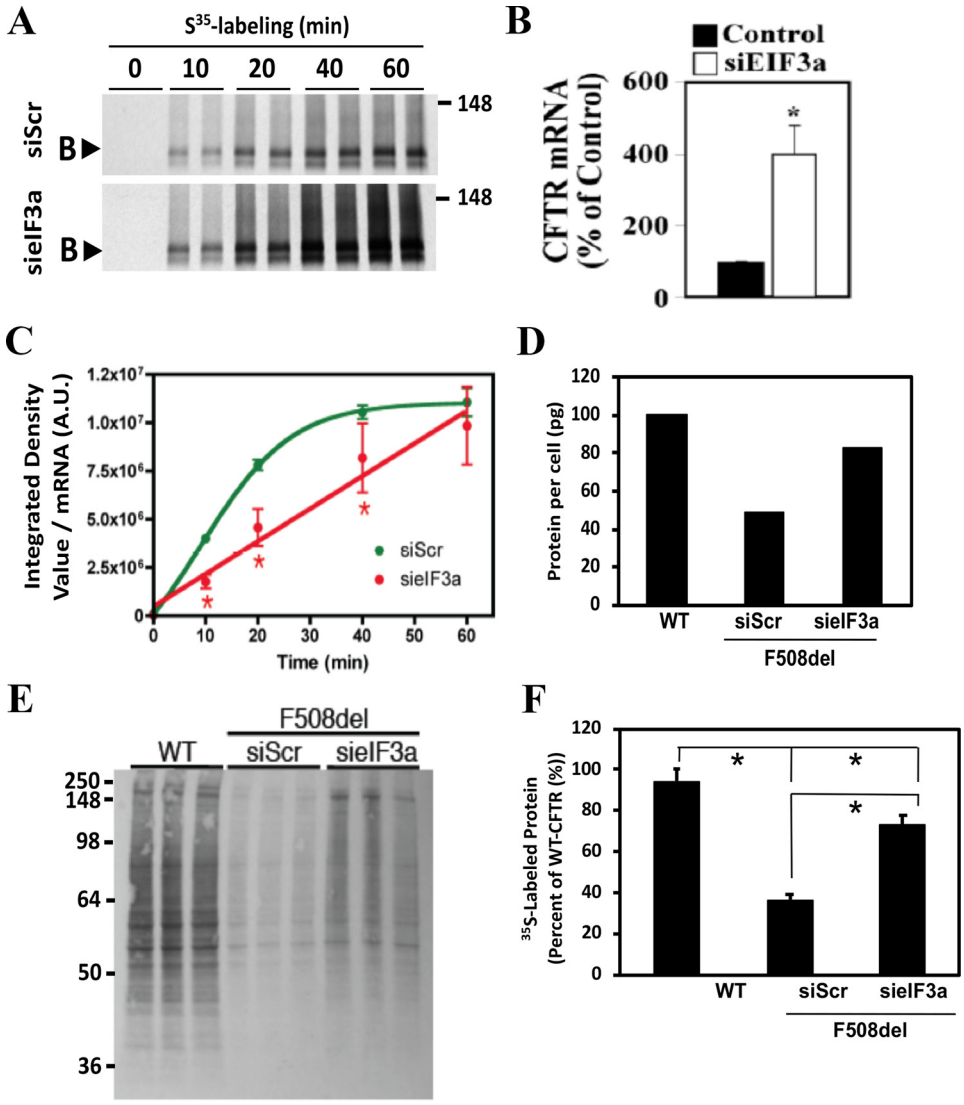

Figure 6. eIF3a silencing reduces the translation rate of F508del. *A,* radiograph of a [^{35}S]Met pulse-labeling time course of F508del-CFTR in response to the treatment of CFBE cells with scramble (*Control*) and eIF3a siRNA. *B,* qRT-PCR of F508del-CFTR levels in F508del-CFTR– expressing cells treated with the indicated siRNA. Results represent a ratio of CFTR to the housekeeping gene, β-glucuronidase, and normalized to control siRNA, which is set to 100% (mean ± S.E., $n \geq 3$, * represents $p < 0.05$ relative to control). *C,* scatter plot analysis of the quantification of the radiogram in *A* normalized to the mRNA levels seen in *B* depicting the rate of CFTR translation in CFBE cells treated with scramble or eIF3a siRNAs. *A.U.* = arbitrary units. *D, histogram* analysis of the total protein per cells in CFBE cells expressing WT-CFTR or F508del-CFTR treated with siScr or eIF3a siRNA. *E,* radiograph of [^{35}S]Met-labeled proteins from CFBE cells expressing WT-CFTR or F508del-CFTR treated with siScr or eIF3a siRNA. *F*, quantitative analysis for the radiograph presented in *E*. Results are shown as percent of WT in each condition (mean ± S.E., $n = 3$; * indicates $p < 0.05$ relative to WT).

passed the level seen upon treatment of F508del-hBE cells with the Food and Drug Administration-approved Vx809 (Fig. 7, *A* and *B*). Moreover, the combined treatment of Vx809 and sheIF3a resulted in a synergistic increase in the amount of band C detected (Fig. 7*B*), indicating that modulation of the expression level of eIF3a provides an important role in amplifying the level of functional F508del under native conditions found in the patient.

In light of the improved trafficking of F508del-CFTR seen in response to the treatment of F508del-hBE cells with sheIF3a alone or in combination with Vx809, we determined whether the corrected F508del-CFTR represented a functional ion channel at the cell surface of primary polarized hBE cells. Short circuit (Isc) measurements of F508del-hBE cells revealed a dose-dependent correction of F508del-CFTR channel activity in response to increasing doses of the sheIF3a-expressing adenovirus (Fig. 7, *C* and *D*), with the m.o.i. of 1000 yielding a forskolin- and genistein-induced current comparable with that seen with Vx809 alone. The combined treatment of VX809 with 500 and 1000 m.o.i. yielded a functional correction of F508del-CFTR to a level reaching 50.1 and 53.6% of the WT-CFTR current measured in hBE primary bronchial epithelia (Fig. 7, *C* and *D*).

These data provide evidence that a modest reduction in the expression level of the translation initiation factor eIF3a provides a substantial corrective benefit for restoration of a Vx809-responsive functional F508del-CFTR at the cell surface of lung epithelial cells, a level that would be predicted to provide significant benefit to patients. The discovery of a prominent role for eIF3a in managing the kinetic assembly of a range of CFTR folding intermediates that are likely differentially impacted by disease-causing variation(s) suggests a role for eIF3-regulated

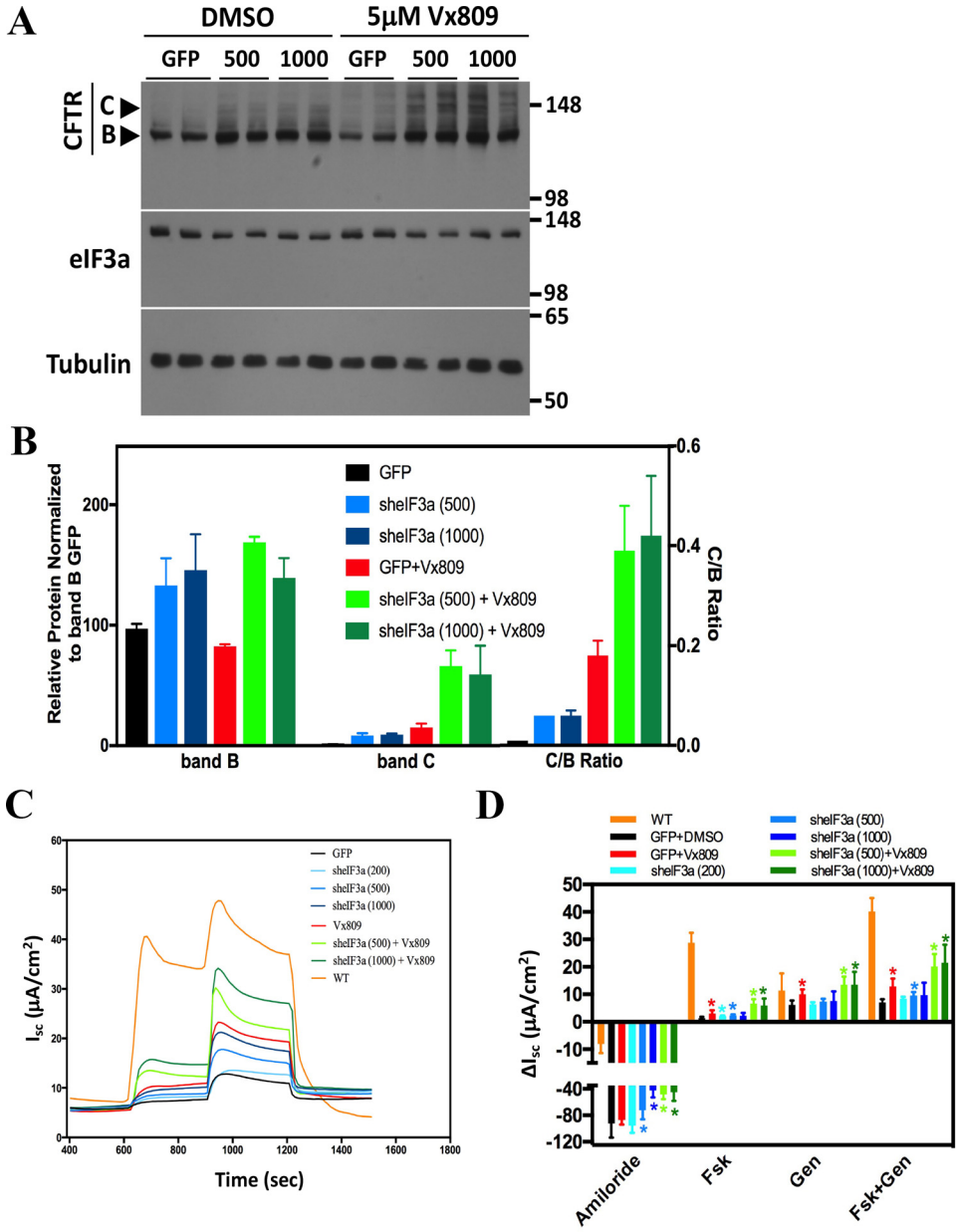

Figure 7. Silencing of EIF3a provides functional correction of F508del-CFTR in primary airway cells. *A,* immunoblot analysis of CFTR, eIF3a, and tubulin in response to the treatment of hBE cells with adenovirally delivered eIF3a shRNA at the indicated m.o.i. alone or in combination with 3 μM Vx809 for 24 h. *B,* quantification of the immunoblot shown in *A*. Data are normalized to the amount of band B glycoform in the GFP control and represent mean ± S.D. ($n = 2$). *C,* representative short-circuit measurement in response to the treatment of hBE cells with adenovirally delivered eIF3a shRNA at the indicated m.o.i. alone or in combination with 3 μM Vx809 for 24 h. *D, histogram* analysis of the amiloride, forskolin (*Fsk*), genistein (*Gen*), and *Fsk* + *Gen*–sensitive currents in hBE cells. Data represent the mean ± S.D. ($n \geq 3$, * indicate $p < 0.05$ relative to F508del-CFTR treated with scramble siRNA).

translational events in generating a functional fold by minimizing the misfolding load imposed by these variants on the prevailing PN of cells.

Discussion

Herein, we utilized a novel integrative proteomic approach to prioritize biological targets for the functional correction of the F508del variant of CFTR, the most common mutation associated with CF. In brief, this method merges two large datasets, namely the siRNA targets that correct F508del-CFTR function and the F508del-CFTR interactome (34), to score high-priority targets that link at least two corrective siRNA hits from the HTS to CFTR ($N_{sp} \geq 2$) while keeping a low randomized connectivity score (N_{rdm}). We refer to these high-priority targets as hub proteins. The method builds upon existing gene prioritization strategies based on topology and network flow (68–70) with NAGA providing two important enhancements as follows: 1) it uses recently available weighted protein interactions gathered from multiple databases, and 2) it includes a randomization procedure to control for input size and composition. Both enhancements aim to improve the specificity of the prioritization relative to the particular set of HTS hits considered within the context of function and cellular organization.

Our novel SPN approach can detect what would appear to be distant connectivities in complex datasets. As an example, we identified eIF3a as a top hub in our network analysis; however, it would only rank 29th in the siRNA HTS hit list had the connection to the CFTR interactome not been considered. This reclassification reflects the clear limitation of omics data when considered alone and out of context of the biology of the cell, emphasizing the challenges in understanding networks when they are disconnected from function (71–76). The prioritization of eIF3a over other siRNA targets, which provided greater YFP quenching in the HTS, is consistent with our pathway enrichment analysis that identified components of the translational pathway as the most enriched in our proteostasis siRNA library screen (Table 3). These data are also consistent with recent observations that the silencing of ribosomal protein L12 (RPL12), which modulates the position of the codon–anticodon recognition site in the ribosome during translational elongation (14, 77), also corrects F508del-CFTR (52). Changes in protein translation associated with alterations in elongation rate have been shown to provide improved folding for diverse proteins in both bacterial and mammalian cells (9, 14, 44, 77). For example, codon optimization experiments have long been used to maximize protein production by increasing the rate of translation and exploiting more abundant tRNAs. However, analyses have shown that whereas the total protein yield does improve, the specific activity of the resulting protein can be decreased (9, 14, 44, 77–79). Moreover, numerous studies have reported that the acceleration of protein translation has deleterious effects on the co-translational folding of proteins, leading to intracellular aggregation and/or degradation (78–87). With respect to F508del, which is a compound mutation of the synonymous codon substitution at Ile-507 (ATT) and the deletion of Phe-508, it has been shown that restoration of the WT Ile-507 codon (ATT to ATC) promoted F508del stabilization by increasing its translation rate, approaching that seen for WT-CFTR (88). The above insights suggest that CFTR variants may require distinct translation programs to overcome both the structural differences in the variant mRNAs and the co-translational folding defect(s) of the variant polypeptides. Although the role of the elongation phase in protein folding is now well-established (14, 16, 44, 77), the identification of a regulatory role for translation initiation proteins, which participate in multiple steps of the translation process, suggests that additional steps might have an impact on the generation of a functionally folded protein. In agreement with this hypothesis, we observed that eIF3a silencing resulted in a decrease in F508del-CFTR production per the mRNA molecule relative to siScr-treated F508del-CFTR– expressing CFBE cells. Although eIF3a has been associated with multiple steps in protein translation, including elongation (46), stop codon recognition (89), and ribosomal recycling (90), its best characterized function remains the assembly of the 48S PIC (9, 11–13, 40–49), leading us to suggest that translation initiation, prior to elongation, can correct F508del-CFTR.

Previously, Wagner *et al.* (43, 48) examined the impact of silencing the individual eIF3 components on the expression profile of the remaining eIF3 proteins as well as assembly of the eIF3 holocomplex. They observed that the silencing of eIF3a leads to a concomitant destabilization of eIF3 proteins found in modules II (eIF3c– e, -k, and -l) and III (eIF3f, -h, and -m) of the holocomplex, without affecting the expression of module I (eIF3b, -g, and -i) or eIF3 accessory proteins (eIF3, eIF2, and eIF5) (43). Although a 60–70% reduction in eIF3a expression resulted in a 85–90% reduction in 43S PIC recovered with the 40S ribosome, only a 40% reduction in RPL41 mRNA binding was observed suggesting the following: 1) the remaining eIF3a can assemble into functional 48S PICs, and 2) the cells adapt to the reduction in available 43S PICs by preferentially translating proteins using monosomes rather than polysomes (Information S4) (43) and adjusts the mRNA levels as needed (Fig. 6*B*) (43). This reduction in the P/M ratio suggests that the availability of functional 43S PIC becomes limiting, resulting in a situation where the elongation/termination time is generally faster than the initiation time leading to an increase in the mRNA pool being translated by monosomes rather than by polysomes (91). Given that the composition of the eIF3 holocomplex remains unchanged (43), despite its reduced levels, it is unlikely that the properties of the eIF3 complex recovered on actively translating ribosomes, as it pertains to elongation (46), termination (89), and ribosome recycling (90), will be altered, suggesting that the impact of eIF3a silencing on generating a functionally folded protein stems from alterations in the initiation rate or frequency. Given that the primary impact of eIF3a silencing results in generating a resource competition for functional ribosomes to initiate the translation process (43), our data suggest that a slowing of the translation initiation rate or a decrease in the number of initiation events on the CFTR mRNA leads to a decreased load of misfolded F508del-CFTR allowing the prevailing PN to better manage the folding requirements of disease-associated variants. The improved folding of F508del-CFTR leads to abrogation of the MSR (Information S5) and its associated reduction in protein expression resulting in the observed increase in F508del stability, trafficking, and function as well as improved global protein expression seen in sieIF3a-treated CFBE and primary hBE cells. These data are in agreement with evidence showing that chemical inhibitors of translation initiation (92) and elongation (52, 92) increase the plasma membrane density, function, and stability of F508del-CFTR and reduce the formation and accumulation of misfolded polypeptides. Indeed, a reduction in translation strategy is frequently used by the unfolded protein response (93) and the integrated stress response (94–96) to regulate the phosphorylation of eIF2α (93, 95, 96), which abruptly terminates translation by preventing release and recycling of ribosomal subunits ultimately resulting in a reduced protein folding burden in the cell (4, 5).

It has been well established that folding efficiency of a protein is affected by mRNA structural elements (97–100) as well as codon usage (101–103), which alter translation elongation rates. However, recent evidence has revealed that structural elements in the 5′-UTR of mRNAs, such as stem-loop structures, untranslated open reading frames (uORFs), and G-quadruplex structures caused by poly(G) stretches, can also affect protein folding efficiency by altering the access of the PIC to the start codon (98). Our data supports a role for the regulation of protein folding through regulation of translation initiation. By

altering the availability of 43S PICs, through a reduction in eIF3a expression, we alter the rate or frequency of translation initiation events on ORFs, leading to a polysome to monosome adaptation in the cells and a subsequent decrease in protein translation. Given that there is a negative correlation in the length of the ORF and ribosome density (104), we suggest that longer mRNAs, such as CFTR, will be particularly disadvantaged in an environment of limited functional ribosomes, leading to an even greater reduction in the expression of these proteins yet resulting in improved folding efficiency.

Although we have previously shown that global protein synthesis is drastically decreased in F508del cells compared with WT (66), little was known regarding which translation factors are involved, how they regulate the *de novo* synthesis and cotranslational folding, or how they can be targeted to correct F508del-CFTR. The siRPL12-mediated correction of F508del-CFTR is consistent with altered translational elongation rates, which may be efficiently coupled to the correct proteostasis components as the polypeptide emerges from the ribosome tunnel (52), generating a stable F508del-CFTR protein. In the context of F508del correction by eIF3a knockdown, a simple explanation is that the reduced availability of 43S PIC to initiate translation of the CFTR variant mRNA may avail the reduced load of nascent polypeptide better access to the chaperone pool to complete folding events that would otherwise fail to be properly completed in the face of increased translation rates or frequency. However, we cannot rule out the possibility that the secondary and tertiary structure of the mRNA, which have now been shown to play a critical role in both initiation and elongation (9, 11–13, 40–49), might be under constant monitoring by the PN to recognize potential challenges of upcoming protein folding events. Variants might fail to properly fold because the thermodynamic requirements of the nascent polypeptide are misinterpreted by the prevailing PN, which fails to properly adjust translation kinetics to match these requirements. This surveillance mechanism could be linked to the nonsense mRNA decay pathway that normally manages dysfunctional mRNA (105–108). Interestingly, although the folding, stability, trafficking, and function of many proteins have been shown to be impacted by alterations in protein translation, the silencing of RPL12 failed to affect other ER-retained proteins such as the Y128S-vasopressin 2 receptor and P92S- and S280L-megalencephalic leukoencephalopathy (MCL1) (52) or, as shown herein, the inability of eIF3a to repair the trafficking defect associated with Z-AAT. These results suggest that the synthesis of misfolded proteins is differentially sensitive to a wealth of relationships that fine-tune translational fidelity. Our work reveals an unanticipated mechanism that could be targeted for the specific management of human variant disease through translation-based therapeutics.

Experimental procedures

Sources of molecular network data

siRNA hits and experimental CFTR interactome data were mapped onto protein interaction networks using HIPPIE version 1.5 (Human integrated Protein–Protein Interaction (109). This database currently contains more than 129,000 interactions of ~14,000 human proteins and is regularly updated by incorporating interaction data from major expert-curated experimental PPI databases (such as BioGRID, HPRD, IntAct, and MINT, total of 10 source databases). It also includes interaction data from 11 experimental studies. All interactions have an associated confidence score based on the sum of cumulative supporting experimental evidence. This score is calculated as a weighted sum of the number of studies in which an interaction was detected, the number and quality of experimental techniques used to measure an interaction, and the number of non-human organisms in which an interaction was reproduced (109). It ranges from 0 to 1, with two predefined confidence levels: medium (0.63–second quartile of the score distribution) or high (0.73–third quartile). For our network construction, we selected a confidence score threshold of 0.5.

Expanded overview of network-augmented genomic analysis

The technique of Network-augmented Genomic Analysis combines high-scoring siRNA hits with a protein interaction network to prioritize key functional proteins and predict novel targets (Fig. 2*A*). Briefly, a list of proteins, including the full siRNA library, the target (CFTR), and the experimentally derived CFTR interactors (CoPIT), is used to seed a human protein–protein interaction network obtained from public databases. In particular, we used the HIPPIE Network Construction tool, within three edges from the seed nodes (maximum allowed by the tool) and a confidence score greater or equal to 0.5 (range 0:1; see below). The resulting graph contained 13,733 unique nodes and 124,567 edges, only slightly smaller than the entire graph available (14,106 nodes and 129,254 edges). We then mapped the high-scoring siRNA hits onto the protein interaction network and computed the shortest paths connecting the sources (siRNA hits) to the target (CFTR) with the Dijkstra's algorithm (51). The Dijkstra algorithm was developed to compute the shortest path between nodes in a graph. This algorithm fixes a single node as the source node and finds the shortest paths from the source to all other nodes in the graph producing a shortest path tree. This step required an undirected, weighted graph where the weights represent distances between the nodes, which are used to calculate the shortest path. In contrast, the edge weights in our graph, obtained from the HIPPIE database, reflect the reliability of combined experimental evidence and are higher for cases with numerous sources of evidence. Thus, we rescored the edge weights to 1) make them compatible with Dijkstra's framework and 2) include interactions between CFTR and CoPIT proteins. The new weights ranged from 0 to 2 and were assigned according to the formula $S = 2 - S_{CoPIT} - S_{db}$, where $S_{CoPIT} = 1$ if and only if the interaction was identified in the CoPIT experiment, and S_{db} equals the HIPPIE confidence score (or 0 if not in the database). Shortest paths computed for each siRNA hit were then aggregated into a (path × path nodes) matrix. The majority of sources had a single path, with few exceptions. For each of the connecting nodes, we computed N_{sp} as the number of paths to distinct siRNA hits (including the node itself, if it is a hit). To filter out nonspecific candidates, the above procedure is repeated for 1000 different sets of sources of the same size of the original set of siRNA hits- drawn randomly without replace-

ment from the entire siRNA library. The resulting distribution of N_{sp} values is then used to compute an average number of paths (N_{rnd}) or each connecting protein in the dataset. Under the hypothesis that highly visited nodes may be important for the biological process under study (*i.e.* CFTR rescue of function), we ranked the connecting proteins based on the number of paths to siRNA hits (N_{sp}) and their specificity to the particular set of high-scoring siRNA hits considered. In particular, we selected proteins with $N_{sp} >= 2$ and ratio $N_{sp}/N_{rnd} > 2$. The false discovery rate of 0.02 for these filtering criteria was computed with 1000 random selections of 369 genes from the siRNA library. Testing for community significance of the subgraph was performed with a Wilcoxon rank-sum test on the internal and external edges incident to the vertices of the subgraph. All graph computations were performed using the R language, the igraph library for network analysis, and Cytoscape for visualization. Functional enrichment analyses were performed with TopGO and WebGestalt.

Cell lines

Human bronchial epithelial cells CFBE41o− stably expressing F508del-CFTR or WT-CFTR were cultured as described previously (57). For temperature-corrected experiments, F508del-CFTR– expressing CFBE cells were transferred to 30 °C for 24 h.

siRNA knockdown and Western blotting

For analysis of CFTR protein and mRNA in response to siRNA-mediated knockdown of eIF targets of interest, cells were seeded at 1.25×10^5 cells per well of a 12-well plate a day prior to transfection and transfected the next day using 50 nM final concentration of siRNA and RNAiMax transfection reagent as per the manufacturer's instructions (Invitrogen). The most potent siRNA target from the 4-siRNA pool in the HTS siRNA library was selected for further analysis. Cells were harvested 72 h after transfection. Preparation of cell lysates and Western blots was done as described previously (57).

qRT-PCR

qRT-PCR was performed using the iScript One-Step RT-PCR kit with SYBR Green (Bio-Rad). RNA was standardized by quantification of glucuronidase (GUS) mRNA, and all values were expressed relative to GUS. Statistical analysis was performed on three independent technical replicates for each RNA sample, where the error bars represent S.E.

Immunoprecipitation (IP), pulse-labeling, and pulse–chase analysis

For each IP, 1 mg of total protein was used. CFTR IP was performed as described previously (31). For total protein synthesis, cells were starved in methionine-free minimum Eagle's medium (Sigma) for 30 min and subsequently pulse-labeled for 1 h with [^{35}S]methionine (0.1 mCi per well in a 6-well plate). Lysates were loaded in a 4–20% gradient gel, with the amount of lysate normalized for number of cells in each condition. CFTR processing efficiency was measured by pulse–chase. Analysis of CFTR stability by pulse–chase was performed as described previously (57). The recovered radiolabeled proteins were then visualized by autoradiography.

CFBE–YFP quenching assay

CFBE41o− cells stably expressing F508del and the halide-sensitive YFP-H148Q/I152L (CFBE–YFP) (50), were reverse-transfected with 50 nM final concentration of an siRNA pool consisting of four siRNAs per target (Dharmacon), and 0.09 μl of Lipofectamine RNAiMax (Invitrogen) per well of a 384-well plates. Cells were trypsinized and suspended in Opti-MEM with 10% FBS, and 6×10^3 cells added per well. Opti-MEM was replaced with growth media 24 h after transfection, and the YFP assay was performed as described previously (110) 72 h after transfection. The HTS screen was performed in triplicate, and hits were validated using the pooled siRNAs and 96-well kinetic YFP quenching assay.

Culturing and adenoviral infection of hBE cells

Primary hBE cells were expanded on PureCol (Advanced BioMatrix)-coated plastic culture plates in bronchial epithelial basal medium (BEBM) supplemented with a bronchial epithelial growth medium bullet kit and 12 μM all-*trans*-retinoic acid until 95% confluent. hBE cells were subsequently transferred to human placental collagen-coated 12-mm Corning Snapwell tissue culture filters at a density of 3.0×10^5 cells per filter and grown in differentiation media (Dulbecco's modified Eagle's medium/F-12 basal medium containing UltroserG, Fetal Clone II, Bovine Brain Extract, 2.5 μg/ml insulin, 20 nM hydrocortisone, 500 nM triiodothreonine, 2.5 μg/ml transferrin, 250 nM ethanolamine, 1.5 μM epinephrine, 250 nM phosphoethanolamine, and 10 nM all-*trans*-retinoic acid) at an air–liquid interface (ALI) for 21–28 days. hBE cells were infected with adenovirus expressing a control or eIF3a shRNA by replacing the basolateral differentiation medium with differentiation medium containing 2 mM EGTA and adding the adenovirus, diluted to the desired multiplicity of infection (m.o.i.) in PBS containing 2 mM EGTA, to the apical side of the Snapwell filter. Cells were incubated at 37 °C, 5% CO_2 for 18 h before removing adenovirus and washing both apical and basolateral sides of the Snapwell filter with PBS and replacing the basolateral differentiation media to EGTA-free differentiation media. Cells were allowed to recover under ALI conditions for 5 days prior to short circuit measurement and Western blot analysis.

Short circuit current measurements

Primary hBE cells were mounted in modified Ussing chambers, and the cultures were continuously short-circuited with an automatic voltage clamp. Transepithelial resistance, R_T, was measured periodically from the current required to apply a 2.5-mV bipolar voltage pulse. R_T was calculated from Ohm's law. The basolateral bathing Ringer solution was composed of 120 mM NaCl, 25 mM $NaHCO_3$, 1.2 mM $CaCl_2$, 1.2 mM $MgCl_2$, 3.3 mM KH_2PO_4, 0.8 mM K_2HPO_4, and 5 mM glucose. NaCl concentration of the apical bathing solution was reduced by replacing NaCl with equimolar sodium gluconate. The chambers were maintained at 37 °C and gassed continuously with a mixture of 95% O_2, 5% CO_2. Sodium currents were blocked by addition of the sodium channel blocker amiloride (10 μM) to

the apical solution. Subsequently, the cAMP agonist, forskolin (10 μM; both chambers), the CFTR potentiator genistein (50 μM; apically), and the CFTR channel blocker CFTRInh-172 (10 μM; apically) were added sequentially to determine cAMP-stimulated CFTR currents.

Data analysis

The data represent densitometric analysis of immunoblots using an Alpha Innotech Fluorochem SP. The quantitation of the Western blots was always normalized to the control (Scramble (Scr)) on their respective blots. The band B in the control (Scramble (siScr)) on each blot is set to 100, allowing the data in each blot to be compared with one another. The error bars represent the standard error of the mean (S.E.) ($n \geq 3$) or the standard deviation of the mean. In all panels, the asterisks indicates a p value < 0.05 as determined by a two-tailed t test using the control as the reference.

Author contributions—D. M. H., S. L., D. M. R., A. I. S., and W. E. B. conceptualization; D. M. H. and D. M. R. data curation; D. M. H., S. L., and D. M. R. formal analysis; D. M. H. and D. M. R. investigation; D. M. H., S. L., D. M. R., and A. I. S. methodology; D. M. H. writing-original draft; D. M. H., S. L., D. M. R., A. I. S., and W. E. B. writing-review and editing; S. L. validation; A. I. S. and W. E. B. supervision; A. I. S. and W. E. B. funding acquisition; A. I. S. and W. E. B. project administration.

References

1. Karczewski, K. J., Weisburd, B., Thomas, B., Solomonson, M., Ruderfer, D. M., Kavanagh, D., Hamamsy, T., Lek, M., Samocha, K. E., Cummings, B. B., Birnbaum, D., The Exome Aggregation Consortium, Daly, M. J., and MacArthur, D. G. (2017) The ExAC browser: displaying reference data information from over 60 000 exomes. *Nucleic Acids Res.* **45,** D840–D845 CrossRef Medline
2. Lek, M., Karczewski, K. J., Minikel, E. V., Samocha, K. E., Banks, E., Fennell, T., O'Donnell-Luria, A. H., Ware, J. S., Hill, A. J., Cummings, B. B., Tukiainen, T., Birnbaum, D. P., Kosmicki, J. A., Duncan, L. E., Estrada, K., *et al.* (2016) Analysis of protein-coding genetic variation in 60,706 humans. *Nature* **536,** 285–291 CrossRef Medline
3. Landrum, M. J., Lee, J. M., Benson, M., Brown, G., Chao, C., Chitipiralla, S., Gu, B., Hart, J., Hoffman, D., Hoover, J., Jang, W., Katz, K., Ovetsky, M., Riley, G., Sethi, A., *et al.* (2016) ClinVar: public archive of interpretations of clinically relevant variants. *Nucleic Acids Res.* **44,** D862–D868 CrossRef Medline
4. Balch, W. E., Morimoto, R. I., Dillin, A., and Kelly, J. W. (2008) Adapting proteostasis for disease intervention. *Science* **319,** 916–919 CrossRef Medline
5. Balchin, D., Hayer-Hartl, M., and Hartl, F. U. (2016) *In vivo* aspects of protein folding and quality control. *Science* **353,** aac4354 CrossRef Medline
6. Li, J., Labbadia, J., and Morimoto, R. I. (2017) Rethinking HSF1 in stress, development, and organismal health. *Trends Cell Biol.* **27,** 895–905 CrossRef Medline
7. Sala, A. J., Bott, L. C., and Morimoto, R. I. (2017) Shaping proteostasis at the cellular, tissue, and organismal level. *J. Cell Biol.* **216,** 1231–1241 CrossRef Medline
8. Labbadia, J., and Morimoto, R. I. (2015) The biology of proteostasis in aging and disease. *Annu. Rev. Biochem.* **84,** 435–464 CrossRef Medline
9. Steffen, K. K., and Dillin, A. (2016) A ribosomal perspective on proteostasis and aging. *Cell Metab.* **23,** 1004–1012 CrossRef Medline
10. Bagdany, M., Veit, G., Fukuda, R., Avramescu, R. G., Okiyoneda, T., Baaklini, I., Singh, J., Sovak, G., Xu, H., Apaja, P. M., Sattin, S., Beitel, L. K., Roldan, A., Colombo, G., Balch, W., *et al.* (2017) Chaperones rescue the energetic landscape of mutant CFTR at single molecule and in cell. *Nat. Commun.* **8,** 398 CrossRef Medline
11. Hinnebusch, A. G. (2006) eIF3: a versatile scaffold for translation initiation complexes. *Trends Biochem. Sci.* **31,** 553–562 CrossRef Medline
12. Hinnebusch, A. G. (2014) The scanning mechanism of eukaryotic translation initiation. *Annu. Rev. Biochem.* **83,** 779–812 CrossRef Medline
13. Hinnebusch, A. G. (2017) Structural insights into the mechanism of scanning and start codon recognition in eukaryotic translation initiation. *Trends Biochem. Sci.* **42,** 589–611 CrossRef Medline
14. Rodnina, M. V., and Wintermeyer, W. (2016) Protein elongation, co-translational folding and targeting. *J. Mol. Biol.* **428,** 2165–2185 CrossRef Medline
15. Thommen, M., Holtkamp, W., and Rodnina, M. V. (2017) Co-translational protein folding: progress and methods. *Curr. Opin. Struct. Biol.* **42,** 83–89 CrossRef Medline
16. Brar, G. A. (2016) Beyond the triplet code: context cues transform translation. *Cell* **167,** 1681–1692 CrossRef Medline
17. Brar, G. A., and Weissman, J. S. (2015) Ribosome profiling reveals the what, when, where and how of protein synthesis. *Nat. Rev. Mol. Cell Biol.* **16,** 651–664 CrossRef Medline
18. Amaral, M. D., and Balch, W. E. (2015) Hallmarks of therapeutic management of the cystic fibrosis functional landscape. *J. Cyst. Fibros.* **14,** 687–699 CrossRef Medline
19. Balch, W. E., Roth, D. M., and Hutt, D. M. (2011) Emergent properties of proteostasis in managing cystic fibrosis. *Cold Spring Harb. Perspect. Biol.* **3,** a004499 Medline
20. Callebaut, I., Chong, P. A., and Forman-Kay, J. D. (2018) CFTR structure. *J. Cyst. Fibros.* **17,** S5–S8 Medline
21. Hartl, D., and Amaral, M. (2015) Cystic fibrosis–from basic science to clinical benefit: a review series. *J. Cyst. Fibros.* **14,** 415–416 CrossRef Medline
22. McClure, M. L., Barnes, S., Brodsky, J. L., and Sorscher, E. J. (2016) Trafficking and function of the cystic fibrosis transmembrane conductance regulator: a complex network of posttranslational modifications. *Am. J. Physiol. Lung Cell Mol. Physiol.* **311,** L719–L733 CrossRef Medline
23. Spielberg, D. R., and Clancy, J. P. (2016) Cystic fibrosis and its management through established and emerging therapies. *Annu. Rev. Genomics Hum. Genet.* **17,** 155–175 CrossRef Medline
24. Brodsky, J. L., and Wojcikiewicz, R. J. (2009) Substrate-specific mediators of ER associated degradation (ERAD). *Curr. Opin. Cell Biol.* **21,** 516–521 CrossRef Medline
25. Vembar, S. S., and Brodsky, J. L. (2008) One step at a time: endoplasmic reticulum-associated degradation. *Nat. Rev. Mol. Cell Biol.* **9,** 944–957 CrossRef Medline
26. Gong, X., Ahner, A., Roldan, A., Lukacs, G. L., Thibodeau, P. H., and Frizzell, R. A. (2016) Non-native conformers of cystic fibrosis transmembrane conductance regulator NBD1 are recognized by Hsp27 and conjugated to SUMO-2 for degradation. *J. Biol. Chem.* **291,** 2004–2017 CrossRef Medline
27. Ahner, A., Gong, X., and Frizzell, R. A. (2016) Divergent signaling via SUMO modification: potential for CFTR modulation. *Am. J. Physiol. Cell Physiol.* **310,** C175–C180 CrossRef Medline
28. Ahner, A., Gong, X., Schmidt, B. Z., Peters, K. W., Rabeh, W. M., Thibodeau, P. H., Lukacs, G. L., and Frizzell, R. A. (2013) Small heat shock proteins target mutant cystic fibrosis transmembrane conductance regulator for degradation via a small ubiquitin-like modifier-dependent pathway. *Mol. Biol. Cell* **24,** 74–84 CrossRef Medline
29. Saxena, A., Banasavadi-Siddegowda, Y. K., Fan, Y., Bhattacharya, S., Roy, G., Giovannucci, D. R., Frizzell, R. A., and Wang, X. (2012) Human heat shock protein 105/110 kDa (Hsp105/110) regulates biogenesis and quality control of misfolded cystic fibrosis transmembrane conductance regulator at multiple levels. *J. Biol. Chem.* **287,** 19158–19170 CrossRef Medline
30. Schmidt, B. Z., Watts, R. J., Aridor, M., and Frizzell, R. A. (2009) Cysteine string protein promotes proteasomal degradation of the cystic fibrosis transmembrane conductance regulator (CFTR) by increasing its interaction with the C terminus of Hsp70-interacting

protein and promoting CFTR ubiquitylation. *J. Biol. Chem.* **284,** 4168–4178 CrossRef Medline

31. Hutt, D. M., Roth, D. M., Chalfant, M. A., Youker, R. T., Matteson, J., Brodsky, J. L., and Balch, W. E. (2012) FK506 binding protein 8 peptidyl-prolyl isomerase activity manages a late stage of cystic fibrosis transmembrane conductance regulator (CFTR) folding and stability. *J. Biol. Chem.* **287,** 21914–21925 CrossRef Medline
32. Tran, J. R., Tomsic, L. R., and Brodsky, J. L. (2011) A Cdc48p-associated factor modulates endoplasmic reticulum-associated degradation, cell stress, and ubiquitinated protein homeostasis. *J. Biol. Chem.* **286,** 5744–5755 CrossRef Medline
33. Ahner, A., Nakatsukasa, K., Zhang, H., Frizzell, R. A., and Brodsky, J. L. (2007) Small heat-shock proteins select δF508-CFTR for endoplasmic reticulum-associated degradation. *Mol. Biol. Cell* **18,** 806–814 CrossRef Medline
34. Pankow, S., Bamberger, C., Calzolari, D., Martínez-Bartolomé, S., Lavallée-Adam, M., Balch, W. E., and Yates, J. R., 3rd. (2015) F508 CFTR interactome remodelling promotes rescue of cystic fibrosis. *Nature* **528,** 510–516 CrossRef Medline
35. Wang, X., Venable, J., LaPointe, P., Hutt, D. M., Koulov, A. V., Coppinger, J., Gurkan, C., Kellner, W., Matteson, J., Plutner, H., Riordan, J. R., Kelly, J. W., Yates, J. R., 3rd., and Balch, W. E. (2006) Hsp90 cochaperone Aha1 downregulation rescues misfolding of CFTR in cystic fibrosis. *Cell* **127,** 803–815 CrossRef Medline
36. Koulov, A. V., LaPointe, P., Lu, B., Razvi, A., Coppinger, J., Dong, M. Q., Matteson, J., Laister, R., Arrowsmith, C., Yates, J. R., 3rd., Balch, W. E. (2010) Biological and structural basis for Aha1 regulation of Hsp90 ATPase activity in maintaining proteostasis in the human disease cystic fibrosis. *Mol. Biol. Cell* **21,** 871–884 CrossRef Medline
37. Solomon, G. M., Raju, S. V., Dransfield, M. T., and Rowe, S. M. (2016) Therapeutic approaches to acquired cystic fibrosis transmembrane conductance regulator dysfunction in chronic bronchitis. *Ann. Am. Thorac Soc.* **13,** Suppl. 2, S169–S176 CrossRef Medline
38. Quon, B. S., and Rowe, S. M. (2016) New and emerging targeted therapies for cystic fibrosis. *BMJ* **352,** i859 Medline
39. Ratjen, F., Bell, S. C., Rowe, S. M., Goss, C. H., Quittner, A. L., and Bush, A. (2015) Cystic fibrosis. *Nat. Rev. Dis. Primers* **1,** 15010 Medline
40. Lacerda, R., Menezes, J., and Romão, L. (2017) More than just scanning: the importance of cap-independent mRNA translation initiation for cellular stress response and cancer. *Cell. Mol. Life Sci.* **74,** 1659–1680 CrossRef Medline
41. Cate, J. H. (2017) Human eIF3: from 'blobology' to biological insight. *Philos. Trans. R. Soc. Lond. B Biol. Sci.* **372,** 20160176 CrossRef Medline
42. Saletta, F., Suryo Rahmanto, Y., and Richardson, D. R. (2010) The translational regulator eIF3a: the tricky eIF3 subunit!. *Biochim. Biophys. Acta* **1806,** 275–286 Medline
43. Wagner, S., Herrmannová, A., Malík, R., Peclinovská, L., and Valášek, L. S. (2014) Functional and biochemical characterization of human eukaryotic translation initiation factor 3 in living cells. *Mol. Cell. Biol.* **34,** 3041–3052 CrossRef Medline
44. Gobet, C., and Naef, F. (2017) Ribosome profiling and dynamic regulation of translation in mammals. *Curr. Opin. Genet. Dev.* **43,** 120–127 CrossRef Medline
45. Valášek, L. S., Zeman, J., Wagner, S., Beznosková, P., Pavlíková, Z., Mohammad, M. P., Hronová, V., Herrmannová, A., Hashem, Y., and Gunišová, S. (2017) Embraced by eIF3: structural and functional insights into the roles of eIF3 across the translation cycle. *Nucleic Acids Res.* **45,** 10948–10968 CrossRef Medline
46. Mohammad, M. P., Munzarová Pondelícková, V., Zeman, J., Gunišová, S., and Valášek, L. S. (2017) *In vivo* evidence that eIF3 stays bound to ribosomes elongating and terminating on short upstream ORFs to promote reinitiation. *Nucleic Acids Res.* **45,** 2658–2674 Medline
47. Lee, A. S., Kranzusch, P. J., and Cate, J. H. (2015) eIF3 targets cell-proliferation messenger RNAs for translational activation or repression. *Nature* **522,** 111–114 CrossRef Medline
48. Wagner, S., Herrmannová, A., Šikrová, D., and Valášek, L. S. (2016) Human eIF3b and eIF3a serve as the nucleation core for the assembly of eIF3 into two interconnected modules: the yeast-like core and the octamer. *Nucleic Acids Res.* **44,** 10772–10788 CrossRef Medline
49. Chiu, W. L., Wagner, S., Herrmannová, A., Burela, L., Zhang, F., Saini, A. K., Valášek, L., and Hinnebusch, A. G. (2010) The C-terminal region of eukaryotic translation initiation factor 3a (eIF3a) promotes mRNA recruitment, scanning, and, together with eIF3j and the eIF3b RNA recognition motif, selection of AUG start codons. *Mol. Cell. Biol.* **30,** 4415–4434 CrossRef Medline
50. Galietta, L. V., Jayaraman, S., and Verkman, A. S. (2001) Cell-based assay for high-throughput quantitative screening of CFTR chloride transport agonists. *Am. J. Physiol. Cell Physiol.* **281,** C1734–C1742 CrossRef Medline
51. Dijkstra, E. (1959) A note on two problems in connexion with graphs. *Numerische Mathematik* **1,** 269–271 CrossRef
52. Veit, G., Oliver, K., Apaja, P. M., Perdomo, D., Bidaud-Meynard, A., Lin, S. T., Guo, J., Icyuz, M., Sorscher, E. J., Hartman, J. L., IV, and Lukacs, G. L. (2016) Ribosomal stalk protein silencing partially corrects the ΔF508-CFTR functional expression defect. *PLoS Biol.* **14,** e1002462 CrossRef Medline
53. LeFebvre, A. K., Korneeva, N. L., Trutschl, M., Cvek, U., Duzan, R. D., Bradley, C. A., Hershey, J. W., and Rhoads, R. E. (2006) Translation initiation factor eIF4G-1 binds to eIF3 through the eIF3e subunit. *J. Biol. Chem.* **281,** 22917–22932 CrossRef Medline
54. Gradi, A., Imataka, H., Svitkin, Y. V., Rom, E., Raught, B., Morino, S., and Sonenberg, N. (1998) A novel functional human eukaryotic translation initiation factor 4G. *Mol. Cell. Biol.* **18,** 334–342 CrossRef Medline
55. Henis-Korenblit, S., Strumpf, N. L., Goldstaub, D., and Kimchi, A. (2000) A novel form of DAP5 protein accumulates in apoptotic cells as a result of caspase cleavage and internal ribosome entry site-mediated translation. *Mol. Cell. Biol.* **20,** 496–506 CrossRef Medline
56. Valášek, L., Phan, L., Schoenfeld, L. W., Valásková, V., and Hinnebusch, A. G. (2001) Related eIF3 subunits TIF32 and HCR1 interact with an RNA recognition motif in PRT1 required for eIF3 integrity and ribosome binding. *EMBO J.* **20,** 891–904 CrossRef Medline
57. Hutt, D. M., Herman, D., Rodrigues, A. P., Noel, S., Pilewski, J. M., Matteson, J., Hoch, B., Kellner, W., Kelly, J. W., Schmidt, A., Thomas, P. J., Matsumura, Y., Skach, W. R., Gentzsch, M., Riordan, J. R., *et al.* (2010) Reduced histone deacetylase 7 activity restores function to misfolded CFTR in cystic fibrosis. *Nat. Chem. Biol.* **6,** 25–33 CrossRef Medline
58. Van Goor, F., Hadida, S., Grootenhuis, P. D., Burton, B., Stack, J. H., Straley, K. S., Decker, C. J., Miller, M., McCartney, J., Olson, E. R., Wine, J. J., Frizzell, R. A., Ashlock, M., and Negulescu, P. A. (2011) Correction of the F508del-CFTR protein processing defect *in vitro* by the investigational drug VX-809. *Proc. Natl. Acad. Sci. U.S.A.* **108,** 18843–18848 CrossRef Medline
59. Bouchecareilh, M., Hutt, D. M., Szajner, P., Flotte, T. R., and Balch, W. E. (2012) Histone deacetylase inhibitor (HDACi) suberoylanilide hydroxamic acid (SAHA)-mediated correction of α1-antitrypsin deficiency. *J. Biol. Chem.* **287,** 38265–38278 CrossRef Medline
60. Perlmutter, D. H., and Silverman, G. A. (2011) Hepatic fibrosis and carcinogenesis in α1-antitrypsin deficiency: a prototype for chronic tissue damage in gain-of-function disorders. *Cold Spring Harb. Perspect. Biol.* **3,** CrossRef Medline
61. Baugh, J. M., and Pilipenko, E. V. (2004) 20S proteasome differentially alters translation of different mRNAs via the cleavage of eIF4F and eIF3. *Mol. Cell* **16,** 575–586 CrossRef Medline
62. Dong, Z., and Zhang, J. T. (2003) EIF3 p170, a mediator of mimosine effect on protein synthesis and cell cycle progression. *Mol. Biol. Cell* **14,** 3942–3951 CrossRef Medline
63. Sha, Z., Brill, L. M., Cabrera, R., Kleifeld, O., Scheliga, J. S., Glickman, M. H., Chang, E. C., and Wolf, D. A. (2009) The eIF3 interactome reveals the translasome, a supercomplex linking protein synthesis and degradation machineries. *Mol. Cell* **36,** 141–152 CrossRef Medline
64. Masutani, M., Sonenberg, N., Yokoyama, S., and Imataka, H. (2007) Reconstitution reveals the functional core of mammalian eIF3. *EMBO J.* **26,** 3373–3383 CrossRef Medline
65. Zhou, M., Sandercock, A. M., Fraser, C. S., Ridlova, G., Stephens, E., Schenauer, M. R., Yokoi-Fong, T., Barsky, D., Leary, J. A., Hershey, J. W.,

Doudna, J. A., and Robinson, C. V. (2008) Mass spectrometry reveals modularity and a complete subunit interaction map of the eukaryotic translation factor eIF3. *Proc. Natl. Acad. Sci. U.S.A.* **105,** 18139–18144 CrossRef Medline

66. Roth, D. M., Hutt, D. M., Tong, J., Bouchecareilh, M., Wang, N., Seeley, T., Dekkers, J. F., Beekman, J. M., Garza, D., Drew, L., Masliah, E., Morimoto, R. I., and Balch, W. E. (2014) Modulation of the maladaptive stress response to manage diseases of protein folding. *PLoS Biol.* **12,** e1001998 CrossRef Medline
67. Chaudhuri, J., Chakrabarti, A., and Maitra, U. (1997) Biochemical characterization of mammalian translation initiation factor 3 (eIF3). Molecular cloning reveals that p110 subunit is the mammalian homologue of *Saccharomyces cerevisiae* protein Prt1. *J. Biol. Chem.* **272,** 30975–30983 CrossRef Medline
68. Berger, B., Peng, J., and Singh, M. (2013) Computational solutions for omics data. *Nat. Rev. Genet.* **14,** 333–346 CrossRef Medline
69. Lan, A., Smoly, I. Y., Rapaport, G., Lindquist, S., Fraenkel, E., and Yeger-Lotem, E. (2011) ResponseNet: revealing signaling and regulatory networks linking genetic and transcriptomic screening data. *Nucleic Acids Res.* **39,** W424–W429 CrossRef Medline
70. Yeger-Lotem, E., Riva, L., Su, L. J., Gitler, A. D., Cashikar, A. G., King, O. D., Auluck, P. K., Geddie, M. L., Valastyan, J. S., Karger, D. R., Lindquist, S., and Fraenkel, E. (2009) Bridging high-throughput genetic and transcriptional data reveals cellular responses to α-synuclein toxicity. *Nat. Genet.* **41,** 316–323 CrossRef Medline
71. Sahni, N., Yi, S., Taipale, M., Fuxman Bass, J. I., Coulombe-Huntington, J., Yang, F., Peng, J., Weile, J., Karras, G. I., Wang, Y., Kovács, I. A., Kamburov, A., Krykbaeva, I., Lam, M. H., Tucker, G., *et al.* (2015) Widespread macromolecular interaction perturbations in human genetic disorders. *Cell* **161,** 647–660 CrossRef Medline
72. Luck, K., Sheynkman, G. M., Zhang, I., and Vidal, M. (2017) Proteome-scale human interactomics. *Trends Biochem. Sci.* **42,** 342–354 CrossRef Medline
73. Rolland, T., Tašan, M., Charloteaux, B., Pevzner, S. J., Zhong, Q., Sahni, N., Yi, S., Lemmens, I., Fontanillo, C., Mosca, R., Kamburov, A., Ghiassian, S. D., Yang, X., Ghamsari, L., Balcha, D., *et al.* (2014) A proteome-scale map of the human interactome network. *Cell* **159,** 1212–1226 CrossRef Medline
74. Yu, M. K., Kramer, M., Dutkowski, J., Srivas, R., Licon, K., Kreisberg, J., Ng, C. T., Krogan, N., Sharan, R., and Ideker, T. (2016) Translation of genotype to phenotype by a hierarchy of cell subsystems. *Cell Syst.* **2,** 77–88 CrossRef Medline
75. Gross, A. M., and Ideker, T. (2015) Molecular networks in context. *Nat. Biotechnol.* **33,** 720–721 CrossRef Medline
76. Carter, H., Hofree, M., and Ideker, T. (2013) Genotype to phenotype via network analysis. *Curr. Opin. Genet. Dev.* **23,** 611–621 CrossRef Medline
77. Rodnina, M. V., Fischer, N., Maracci, C., and Stark, H. (2017) Ribosome dynamics during decoding. *Philos. Trans. R. Soc. Lond. B Biol. Sci.* **372,** 20160182 CrossRef Medline
78. Fedyunin, I., Lehnhardt, L., Böhmer, N., Kaufmann, P., Zhang, G., and Ignatova, Z. (2012) tRNA concentration fine tunes protein solubility. *FEBS Lett.* **586,** 3336–3340 CrossRef Medline
79. Komar, A. A., Lesnik, T., and Reiss, C. (1999) Synonymous codon substitutions affect ribosome traffic and protein folding during in vitro translation. *FEBS Lett.* **462,** 387–391 CrossRef Medline
80. Chadani, Y., Niwa, T., Chiba, S., Taguchi, H., and Ito, K. (2016) Integrated *in vivo* and *in vitro* nascent chain profiling reveals widespread translational pausing. *Proc. Natl. Acad. Sci. U.S.A.* **113,** E829–E838 CrossRef Medline
81. Kim, S. J., Yoon, J. S., Shishido, H., Yang, Z., Rooney, L. A., Barral, J. M., and Skach, W. R. (2015) Protein folding. Translational tuning optimizes nascent protein folding in cells. *Science* **348,** 444–448 CrossRef Medline
82. Morgunov, A. S., and Babu, M. M. (2014) Optimizing membrane-protein biogenesis through nonoptimal-codon usage. *Nat. Struct. Mol. Biol.* **21,** 1023–1025 CrossRef Medline
83. Pechmann, S., Chartron, J. W., and Frydman, J. (2014) Local slowdown of translation by nonoptimal codons promotes nascent-chain recognition by SRP *in vivo*. *Nat. Struct. Mol. Biol.* **21,** 1100–1105 CrossRef Medline
84. Siller, E., DeZwaan, D. C., Anderson, J. F., Freeman, B. C., and Barral, J. M. (2010) Slowing bacterial translation speed enhances eukaryotic protein folding efficiency. *J. Mol. Biol.* **396,** 1310–1318 CrossRef Medline
85. Spencer, P. S., Siller, E., Anderson, J. F., and Barral, J. M. (2012) Silent substitutions predictably alter translation elongation rates and protein folding efficiencies. *J. Mol. Biol.* **422,** 328–335 CrossRef Medline
86. Bäuerlein, F. J. B., Saha, I., Mishra, A., Kalemanov, M., Martínez-Sánchez, A., Klein, R., Dudanova, I., Hipp, M. S., Hartl, F. U., Baumeister, W., and Fernández-Busnadiego, R. (2017) *In situ* architecture and cellular interactions of polyQ inclusions. *Cell* **171,** 179–187.e10 CrossRef Medline
87. Hartl, F. U. (2017) Protein misfolding diseases. *Annu. Rev. Biochem.* **86,** 21–26 CrossRef Medline
88. Bartoszewski, R. A., Jablonsky, M., Bartoszewska, S., Stevenson, L., Dai, Q., Kappes, J., Collawn, J. F., and Bebok, Z. (2010) A synonymous single nucleotide polymorphism in ΔF508 CFTR alters the secondary structure of the mRNA and the expression of the mutant protein. *J. Biol. Chem.* **285,** 28741–28748 CrossRef Medline
89. Beznosková, P., Cuchalová, L., Wagner, S., Shoemaker, C. J., Gunišová, S., von der Haar, T., and Valášek, L. S. (2013) Translation initiation factors eIF3 and HCR1 control translation termination and stop codon read-through in yeast cells. *PLoS Genet.* **9,** e1003962 CrossRef Medline
90. Pisarev, A. V., Hellen, C. U., and Pestova, T. V. (2007) Recycling of eukaryotic posttermination ribosomal complexes. *Cell* **131,** 286–299 CrossRef Medline
91. Heyer, E. E., and Moore, M. J. (2016) Redefining the translational status of 80S monosomes. *Cell* **164,** 757–769 CrossRef Medline
92. Meriin, A. B., Mense, M., Colbert, J. D., Liang, F., Bihler, H., Zaarur, N., Rock, K. L., and Sherman, M. Y. (2012) A novel approach to recovery of function of mutant proteins by slowing down translation. *J. Biol. Chem.* **287,** 34264–34272 CrossRef Medline
93. Walter, P., and Ron, D. (2011) The unfolded protein response: from stress pathway to homeostatic regulation. *Science* **334,** 1081–1086 CrossRef Medline
94. Pakos-Zebrucka, K., Koryga, I., Mnich, K., Ljujic, M., Samali, A., and Gorman, A. M. (2016) The integrated stress response. *EMBO Rep.* **17,** 1374–1395 CrossRef Medline
95. Sekine, Y., Zyryanova, A., Crespillo-Casado, A., Fischer, P. M., Harding, H. P., and Ron, D. (2015) Stress responses. Mutations in a translation initiation factor identify the target of a memory-enhancing compound. *Science* **348,** 1027–1030 CrossRef Medline
96. Pavitt, G. D., and Ron, D. (2012) New insights into translational regulation in the endoplasmic reticulum unfolded protein response. *Cold Spring Harb. Perspect. Biol.* **4,** CrossRef
97. Churbanov, A., Rogozin, I. B., Babenko, V. N., Ali, H., and Koonin, E. V. (2005) Evolutionary conservation suggests a regulatory function of AUG triplets in 5′-UTRs of eukaryotic genes. *Nucleic Acids Res.* **33,** 5512–5520 CrossRef Medline
98. Dacheux, E., Malys, N., Meng, X., Ramachandran, V., Mendes, P., and McCarthy, J. E. G. (2017) Translation initiation events on structured eukaryotic mRNAs generate gene expression noise. *Nucleic Acids Res.* **45,** 6981–6992 CrossRef Medline
99. Faure, G., Ogurtsov, A. Y., Shabalina, S. A., and Koonin, E. V. (2016) Role of mRNA structure in the control of protein folding. *Nucleic Acids Res.* **44,** 10898–10911 CrossRef Medline
100. Jia, M., and Luo, L. (2006) The relation between mRNA folding and protein structure. *Biochem. Biophys. Res. Commun.* **343,** 177–182 CrossRef Medline
101. Boël, G., Letso, R., Neely, H., Price, W. N., Wong, K. H., Su, M., Luff, J., Valecha, M., Everett, J. K., Acton, T. B., Xiao, R., Montelione, G. T., Aalberts, D. P., and Hunt, J. F. (2016) Codon influence on protein expression in *E. coli* correlates with mRNA levels. *Nature* **529,** 358–363 CrossRef Medline
102. Shabalina, S. A., Spiridonov, N. A., and Kashina, A. (2013) Sounds of silence: synonymous nucleotides as a key to biological regulation and complexity. *Nucleic Acids Res.* **41,** 2073–2094 CrossRef Medline
103. Zhao, F., Yu, C. H., and Liu, Y. (2017) Codon usage regulates protein structure and function by affecting translation elongation speed in *Drosophila* cells. *Nucleic Acids Res.* **45,** 8484–8492 CrossRef Medline

104. Fernandes, L. D., Moura, A. P. S., and Ciandrini, L. (2017) Gene length as a regulator for ribosome recruitment and protein synthesis: theoretical insights. *Sci. Rep.* **7,** 17409 CrossRef Medline
105. Sesen, J., Casaos, J., Scotland, S. J., Seva, C., Eisinger-Mathason, T. S., and Skuli, N. (2017) The bad, the good and eIF3e/INT6. *Front. Biosci.* **22,** 1–20 CrossRef Medline
106. Raxwal, V. K., and Riha, K. (2016) Nonsense mediated RNA decay and evolutionary capacitance. *Biochim. Biophys. Acta* **1859,** 1538–1543 CrossRef Medline
107. Kurosaki, T., and Maquat, L. E. (2016) Nonsense-mediated mRNA decay in humans at a glance. *J. Cell Sci.* **129,** 461–467 CrossRef Medline
108. Lykke-Andersen, S., and Jensen, T. H. (2015) Nonsense-mediated mRNA decay: an intricate machinery that shapes transcriptomes. *Nat. Rev. Mol. Cell Biol.* **16,** 665–677 CrossRef Medline
109. Alanis-Lobato, G., Andrade-Navarro, M. A., and Schaefer, M. H. (2017) HIPPIE v2.0: enhancing meaningfulness and reliability of protein-protein interaction networks. *Nucleic Acids Res.* **45,** D408–D414 CrossRef Medline
110. Calamini, B., Silva, M. C., Madoux, F., Hutt, D. M., Khanna, S., Chalfant, M. A., Saldanha, S. A., Hodder, P., Tait, B. D., Garza, D., Balch, W. E., and Morimoto, R. I. (2011) Small-molecule proteostasis regulators for protein conformational diseases. *Nat. Chem. Biol.* **8,** 185–196 CrossRef Medline